Materials Today Bio 29 (2024) 101282

Contents lists available at ScienceDirect

Materials Today Bio

journal homepage: www.journals.elsevier.com/materials-today-bio

Simultaneous targeting and suppression of heat shock protein 60 to overcome heat resistance and induce mitochondrial death of tumor cells in photothermal immunotherapy

Yiling Meng [a], Tao Wen [a,**], Xuanxin Liu [a], Aiyun Yang [b], Jie Meng [a], Jian Liu [a], Jianhua Wang [b], Haiyan Xu [a,*]

[a] Institute of Basic Medical Sciences, Chinese Academy of Medical Sciences & School of Basic Medicine, Peking Union Medical College, Beijing, 100005, China
[b] Translational Medicine Laboratory, Beijing Key Laboratory of Child Development and Nutriomics, Capital Institute of Pediatrics, Beijing, 100020, China

ARTICLE INFO

Keywords:
HSP60
Gold nanorods
Mitochondrial targeting
Photothermal therapy
Triple-negative breast cancer

ABSTRACT

As the most aggressive and metastatic subtype of breast cancer, clinical demands of triple negative breast cancer (TNBC) have far not been met. Heat shock protein 60 (HSP60) is over expressed in tumor cells and impair the efficacy of photothermal therapy. In this work, a conjugate composed of self-designed peptide targeting HSP60 and gold nanorods was constructed, referred to as AuNR-P17. Results showed that AuNR-P17 was able to simultaneously down regulate the level of HSP60 and locate in the mitochondria where HSP60 is enriched in the tumor cells of TNBC, which also impeded the interaction between HSP60 and integrin α_3, thereby reducing the tumor cells' heat tolerance and metastatic capabilities. At the same time, AuNR-P17 induced remarkable mitochondrial apoptosis when exposed to the laser irradiation of 808 nm. The dual functions of AuNR-P17 led to the decrement of BCL-2 and the activation of p53 and cleaved caspase-3. The danger associated molecular patterns (DAMPs) generated from the mitochondrial apoptosis elicited strong and long-term specific immune responses against TNBC *in vivo* and ultimately inhibited the tumor metastasis and recurrence with significantly prolonged survival (>100 days) on TNBC mice. In conclusion, this study demonstrated HSP60 a promising potential therapeutic target for triple negative breast cancer and exhibited powerful capacity of AuNR-P17 in photothermal immune therapy.

1. Introduction

Breast cancer is one of the most commonly diagnosed cancers and leading cause of cancer death in women [1]. It has been well known that surgery, radiotherapy, chemotherapy, and targeted therapy are major treatments of breast cancer [2]. Although targeted treatments have made great progress [3], unfortunately, triple negative breast cancer (TNBC) benefits little from existing targeted therapeutics because this subtype does not have those well-known specific targets [4,5], meanwhile, TNBC is the most aggressive and metastatic subtype of breast cancer. Therefore, clinical demands of TNBC have far not been met [6].

Although photothermal therapies (PTT) for TNBC have garnered considerable research attention, an important factor that significantly impairs the therapeutic efficacy is heat shock proteins (HSPs) generating along with PTT. HSPs increase when cells are suffered laser irradiation [7–9], helping tumor cells more tolerant to hyperthermia and consequently reducing the efficacy of PTT [10–12]. In addition, it has been recognized that the efficacy of PTT largely depends on the localization of the photothermal reagents in specific organelles [13]. Notably, mitochondrion-localized phototherapy has been proven to be particularly effective in eliminating cancer cells, exhibiting significant efficacy in cancer eradication [14], which are mainly achieved by conjugating triphenyl-phosphonium (TPP) or its analogues to nanoparticles [15–18], and other approaches include the applications of mitochondrial-localization sequence that can be specifically cleaved by mitochondrial matrix peptidase [19] and a variant of turbo green fluorescent protein (mitoTGFP) [20].

Among various HSPs, HSP60 is over expressed in breast cancer patients' tissue and cells, especially in TNBC [21]. HSP60 plays an important role in protein folding, assembly, and transportation, and is

* Corresponding author.
** Corresponding author.
E-mail addresses: went@ibms.pumc.edu.cn (T. Wen), xuhy@pumc.edu.cn (H. Xu).

https://doi.org/10.1016/j.mtbio.2024.101282
Received 1 August 2024; Received in revised form 23 September 2024; Accepted 27 September 2024
Available online 29 September 2024

closely related to the occurrence and development of various tumors, implying its valuable potential as a therapeutic target for TNBC [22,23]. Notably, HSP60 is over expressed both in the tumor cells membrane and stores in the mitochondria [24], the unique location offers a compelling opportunity to simultaneously inhibit the function of HSP60 and target TNBC cells and their mitochondria.

Herein, an HSP60 targeted peptide (P17), developed in our previous work [25], was conjugated to gold nanorods in a single-step procedure. The conjugate, referred to as AuNR-P17, was investigated in the triple-negative breast cancer tumor cells and murine model. Here we showed that AuNR-P17 was able to simultaneously down regulate the level of HSP60 and locate in the mitochondria where HSP60 is enriched in the tumor cells of TNBC, inducing remarkable mitochondrial apoptosis when exposed to the laser irradiation of 808 nm. The dual functions of AuNR-P17 led to strong and long-term specific immune responses against TNBC *in vivo* and ultimately inhibited the tumor metastasis and recurrence with significantly prolonged survival of the tumor-bearing mice, which demonstrated HSP60 a promising potential therapeutic target for TNBC and exhibited powerful capacity of AuNR-P17 in photothermal immune therapy.

2. Methods and materials

2.1. Chemical reagents

Sigma-Aldrich was the source of Sodium borohydride ($NaBH_4$), chlorauric acid ($HAuCl_4{\cdot}3H_2O$), cetyltrimethylammonium bromide (CTAB), sodium citrate, silver nitrate ($AgNO_3$), L-ascorbic acid (AA), sodium polystyrene sulfonate (PSS) and 2',7'-dichlorofluorescein diacetate (DCFH-DA). Milli-Q water (18 MΩ cm) was used for solution preparation. Hyclone Laboratories provided Modified RPMI medium, DMEM high glucose medium, trypsin, penicillin-streptomycin. Gibco provided fetal bovine serum (FBS). Dojindo Molecular Technologies provided CCK-8 kit, LDH detection kit and propidium iodide (PI). Beyotime biotechnology provided the adenosine 5′-triphosphate (ATP) bioluminescent assay kit and cytochrome C (Cyto C) antibody, and Chondrex provided the high mobility group box 1 (HMGB1) detection kit. Abcam provided the HSP60 Elisa kit and calreticulin (CRT) rabbit mAb, while Cell Signaling Technology provided the HSP60 (D6F1) XP® Rabbit mAb. Integrin alpha 3 polyclonal antibody, CoraLite®488-conjugated affinipure goat anti-rabbit IgG and CoraLite®594-conjugated HSP60 monoclonal antibody were purchased from proteintech. Mito-Tracker Red CMXRos was purchased from Thermo Fisher Scientific, and TNF-α and IFN-γ Elisa kits were purchased from Neobioscience. The mouse splenic lymphocyte isolation kit was purchased from Tian Jin Hao Yang Biological Manufacture Co., LTD (China). All reagents and solvents were of analytical grade and used without further purification.

2.2. AuNRs synthesis process

A regular seed-mediated growth method was employed to synthesize PSS-coated gold nanorods (AuNRs) [26]. Initially, $HAuCl_4$ (103 μL, 24.28 mM) was reduced with $NaBH_4$ through a chemical reduction process, in the presence of CTAB (7.5 mL, 0.1 M) and diluted with deionized water to 9.4 mL. Upon the addition of ice-cold $NaBH_4$ (0.6 mL, 0.01 M) and magnetic stirring, Au seeds were formed, and the solution color changed to brown. The Au seeds were utilized within 2–5 h, kept at 30 °C. To prepare the AuNRs, a growth solution comprising of CTAB (500 mL, 0.1 M), $HAuCl_4$ (10.3 mL, 24.28 mM), $AgNO_3$ (3.4 mL, 10 mM), H_2SO_4 (5 mL, 1 M), and AA (4 mL, 0.1 M) was employed, followed by the addition of seed solution (1.2 mL) to initiate AuNRs growth at a constant temperature of 30 °C. After 12 h, centrifugation was performed twice at 12000 rpm for 5 min to purify the AuNRs, which were then coated with PSS (the volume ratio of AuNRs to PSS is 20:1) for another 12 h. The resulting precipitate was collected and redispersed in deionized water and the solution was stored at 4 °C.

2.3. Preparation of AuNR-P17

Peptide P17 (GDQNLQGPMLQGDPGFQRCIDGNVRLVFLFRGKKK KKKG, 98 % purity) was chemically synthesized by Guoping Pharmaceutical Co., Ltd (Anhui, China). The synthesis of AuNR-P17 was executed via incubation of a FITC-labeled P17 solution with AuNRs. Specifically, a concentration of 4 μM P17 was allowed to react with 1.36 μM AuNRs at 30 °C for 8 h. Subsequently, excess P17 was eliminated through centrifugation (10000 rpm, 5 min), and the resulting precipitate was resuspended using deionized water. The AuNR-P17 solution was then stored at 4 °C until utilization.

2.4. The characterization of AuNRs and AuNR-P17

The morphological features of the AuNR-P17 solution were examined via TEM (TEM-1400 plus, JEOL Ltd, Tokyo, Japan) on a copper net. To prepare the suspended dispersions, 10 μL of nanorods were mixed with 990 μL of ddH_2O. The nanorods were quantified using UV–vis–NIR spectroscopy (Lamdba 950, Perkin Elmer). The solution's zeta potential was determined using dynamic light scattering (DLS, Nano ZS90 Zetasizer, Malvern Instruments, Malvern, UK). FT-IR spectroscopy was performed using a Perkin Elmer Frontier, with CCl_4 being used to precipitate the samples. Additionally, XPS measurement was carried out via Thermo Scientific K-Alpha at Shiyanjia lab (www.Shiyanjia.com).

2.5. Cell culture

The mouse breast cancer 4T1 cell line was procured from Cell Bank of Shanghai Institutes of Biological Sciences, Chinese Academy of Sciences (Shanghai, China), while the mouse melanoma B16-F10 cell line were purchased from the Cell Resource Center of the Chinese Academy of Medical Sciences (Beijing, China). DC2.4 cell line was generously provided by Prof. Lanxia Liu (Institute of Biomedical Engineering, Chinese Academy of Medical Sciences & Peking Union Medical College). The cells were cultured in modified RPMI medium containing 10 % FBS, 100 U/mL of penicillin and 100 μg/mL of streptomycin for 4T1, and DC2.4 cells, while B16-F10 cells were cultured in DMEM high glucose medium supplemented with 10 % FBS, 100 U/mL penicillin and 100 μg/mL streptomycin. All cells were maintained at 37 °C in a cell incubator containing 5 % CO_2.

2.6. HSP60 expression and binding detection

4T1 cells were seeded in a 175 cm^2 bottle with 1×10^7 cells for 24 h, collected, washed. the half cells were fixed and permeabilized, while the other half remained untreated. Cells were incubated with anti-HSP60 antibody, washed with phosphate buffered saline (PBS), and incubated with Alexa Fluor 647-conjugated secondary antibody to assess HSP60 expression by flow cytometry. Separately, 4T1 cells were seeded in 24-well plates at 1×10^5 cells/well for 24 h. Cells were cultured with nanorods at 40 μg/mL for another 24 h, collected, and washed. The binding ability of cells with AuNR-P17 was measured by detecting the FITC fluorescence intensity of P17.

2.7. Cellular uptake assay

4T1 cells were seeded in 96-well plates at a density of 1×10^4 cells per well and allowed to incubate for 24 h. Then nanorods were introduced to the culture system at 40 μg/mL and incubated for an additional 24 h. Subsequently, the solution was removed, and the cells were washed with PBS. The extinction spectra of the cells in each group were measured to assess the extent of nanorod uptake by subtracting the extinction spectra of cells without any treatment.

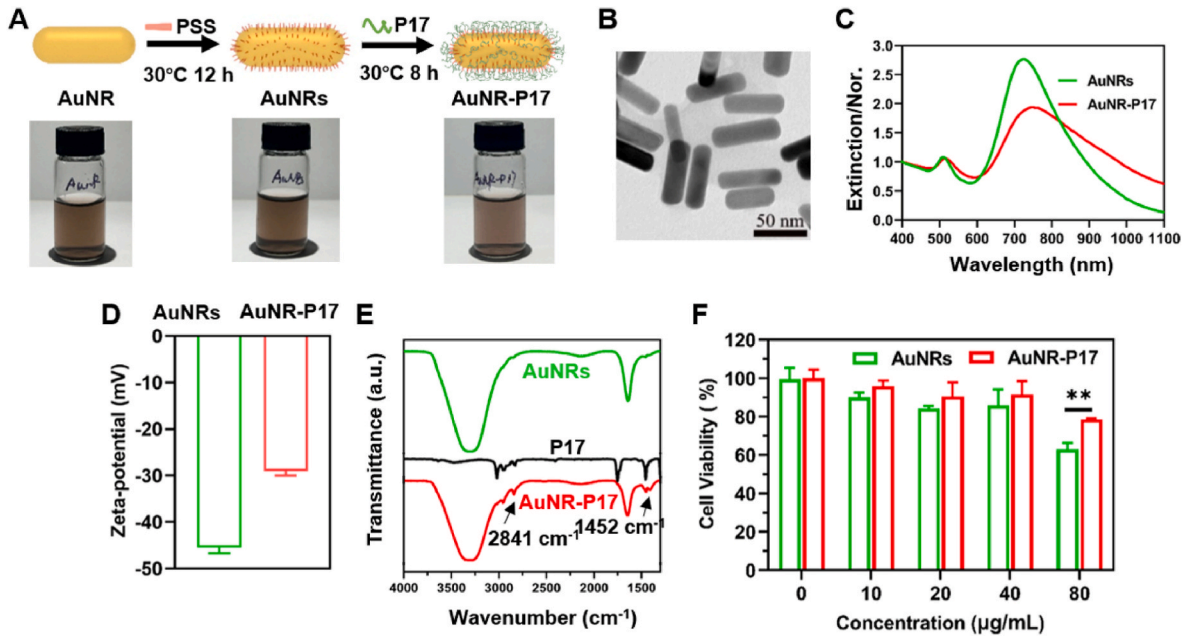

Fig. 1. Characterizations of different nanorods. (A) Diagram for fabrication of AuNR-P17 and corresponding photos of nanorods solution. (B) Transmission Electron Microscope (TEM) image of AuNR-P17. (C) UV–vis–NIR extinction spectra of nanorods normalized at 400 nm. (D) Zeta potential and (E) FT-IR spectrum of nanorods. (F) Relative viability of 4T1 cells incubated with nanorods for 24 h measured by CCK-8 assay (n = 3).

2.8. Cytotoxicity assay

4T1 were cultured in 96-well plates at a seeding density of 1×10^4 cells per well for 24 h and incubated with various concentrations of nanorod solutions (10, 20, 40, and 80 μg/mL) for another 24 h. Afterward, 4T1 cells were washed with PBS for subsequent CCK-8 assay following the recommended protocol. For the temperature measuring, the cell culture medium was refreshed with PBS and the cells were irradiated with laser (808 nm, 2.0 W/cm^2) for 1 or 2 min. The negative control group was that without any treatments. Thermoelectric coupling was utilized to monitor the temperature of the cells in each group. All the cells were subjected to the CCK-8 kit.

2.9. Dead cell staining assay

After treatment with/without laser for 2 min (2.0 W/cm^2), cells were incubated with PI solutions (8 μM) in PBS buffer for 5 min. Subsequently, the cells were washed with PBS and observed using confocal laser scanning microscopy (CLSM; Olympus, IX53). PI was excited with a laser at 543 nm.

2.10. Synchrotron radiation-based soft X-ray nanocomputed tomography (nano-CT)

The 100 mesh nickel mesh (face up, Beijing Zhongjingkeyi Technology Co., China) was placed at the bottom of the 96-well plate, and 4T1 cells (2×10^3/well) with logarithmic growth phase were added to the well overnight, and 40 μg/mL of AuNR-P17 was added and incubated for 24 h. Remove the nickel mesh, wash it with PBS, gently put it in 4 % paraformaldehyde (fixed) for 2 h, change the paraformaldehyde into PBS solution (kept in liquid). The cells, which had been washed with deionized water, were immediately subjected to rapid freezing in liquid nitrogen. Subsequently, the sample was moved to the primary chamber for cryoimaging via the transfer chamber. The three-dimensional (3D) cryo-soft X-ray imaging experiments were conducted at beamline BL07W of the National Synchrotron Radiation Laboratory in Hefei, China. The X-ray beam was focused onto the sample using an elliptical capillary condenser. A magnified image of the sample was generated on a 166-bit 1024 × 1024 charge-coupled device camera with a 12-μm field of view and a spatial resolution of 30 nm by the objective zone plate. To construct the 3D volume, a tilt series comprising 235 images taken at 1° intervals was acquired at X-ray energy of 520 eV. Each projection was captured with an exposure time of 2 s. Segmentation and rendering were performed using Avizo 2019.1.

2.11. Mitochondrial staining

To confirm whether AuNR-P17 locates in 4T1 mitochondria, we stained mitochondria of 4T1 cells. 4T1 cells were seeded on the glass slide in 24-well plates to prepare the cell slide at a density of 5×10^4 cells per well for 12 h and incubated with nanorods at 40.0 μg/mL for 24 h. After washing with PBS three times, cells were incubated with 250 nM MitoTracker Red CMXRos for 30 min to stain the cell mitochondria, then washed with PBS for three times and fixed with 3.7 % formaldehyde for 15 min. After washed with PBS for another three times, the nuclei were stained blue with DAPI sealing tablets. The cells without any treatment were set as the control.

2.12. TEM

To observe the distribution of nanorods in organelles when incubated with nanorods at different time points, the TEM of cells was conducted. 4T1 cells were seeded in 75 cm^2 culture bottle with 1×10^6 cells for 24 h and incubated with nanorods at 40.0 μg/mL for 24 h. The cells were washed with PBS and collected by a cell scraper. After centrifugation (1500 rpm, 5min), 2.5 % glutaraldehyde was slowly added to fix the cells and the cells were placed in a refrigerator at 4 °C overnight. The fixative solution was poured out and the sample was rinsed with 0.1M phosphoric acid buffer (pH 7.0) three times. The sample was fixed with 1 % osmium solution for 1–2 h. After necessary treated, the samples were sliced in an ultra-thin slicing machine to obtain sections of 70–90 nm. The sections were stained with lead citrate solution and uranium dioxy acetate 50 % ethanol saturated solution for 5–10 min each. After drying, the samples were observed with TEM.

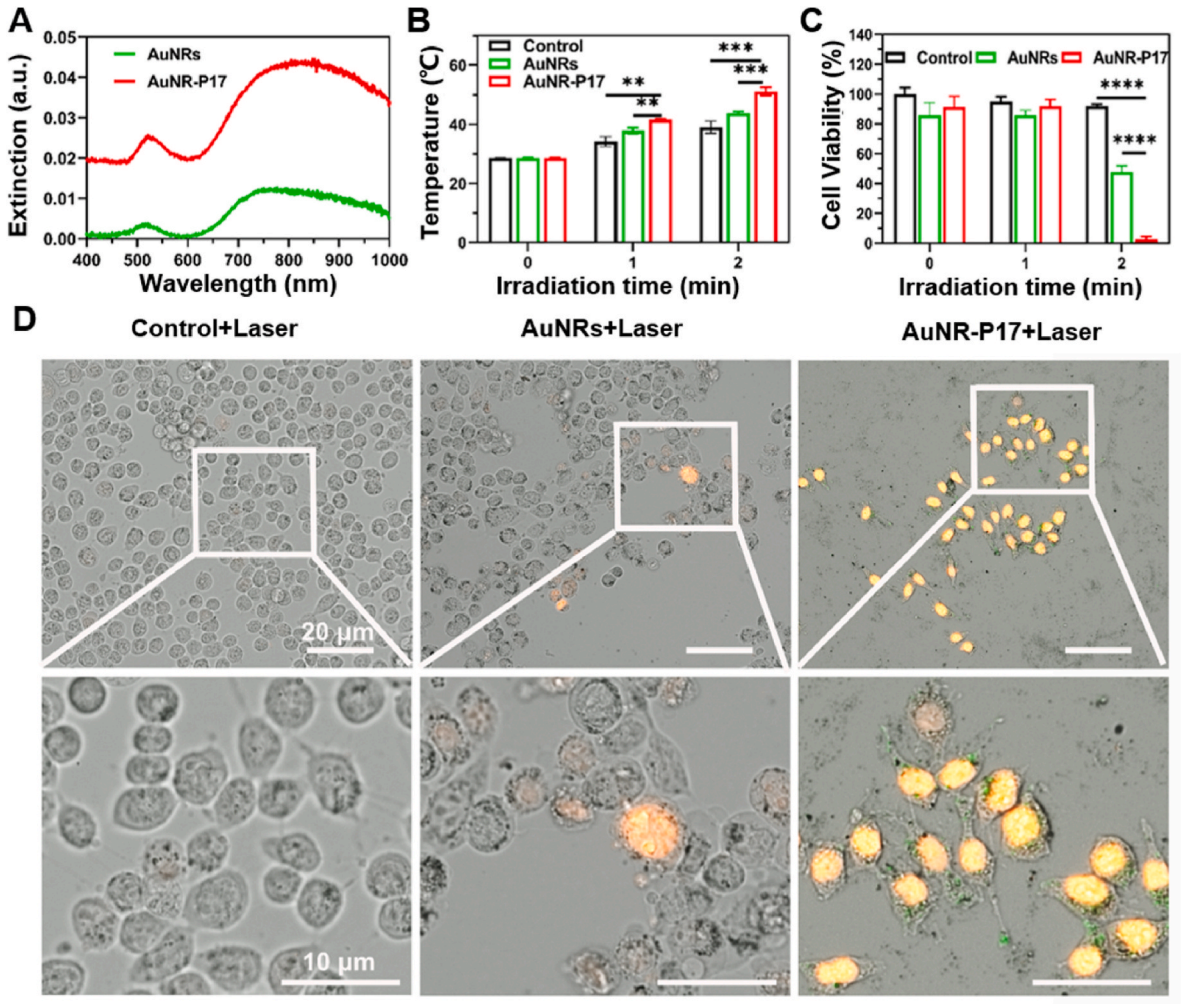

Fig. 2. Photothermal effects on cell viability induced by AuNR-P17 with laser irradiation of 808 nm. (A) Extinction spectra of cells incubated with AuNRs and AuNR-P17 at 40 μg/mL for 24 h. (B) The temperature of solution for cells incubated with AuNRs and AuNR-P17 at 40 μg/mL for different irradiation period of 808 nm of 2.0 W/cm^2 (n = 3). (C) The relative cell viability measured by CCK-8 assay. The cells were incubated with AuNRs and AuNR-P17 followed by laser irradiation of 808 nm of 2.0 W/cm^2 for 1 min and 2 min (n = 3). (D) Representative fluorescent images merged with bright field for 4T1 cells irradiated with 808 nm laser at 2.0 W/cm^2 for 2 min following AuNRs and AuNR-P17 incubation for 24 h. Yellow fluorescence was merged by red of dying cell staining with PI and green of FITC-labeled P17.

2.13. Release of cyto C

After overnight culture of 4T1 cells in RPMI medium, cells were treated with 40 μg/mL AuNRs or AuNR-P17 for 24 h. They were then irradiated for 2 min with or without 2.0 W/cm^2. Cells were fixed with 4 % formaldehyde for 2 min, washed twice with PBS for 5 min each, and incubated with 5 % BSA at room temperature for 1 h. Cytochrome C antibody was diluted 1:50 with primary antibody diluent, incubated overnight, and washed three times with PBS for 5 min each. Secondary antibodies, diluted 1:75 (red), were incubated at room temperature for 1 h with gentle shaking, followed by three washes with PBS. Cells were stained with Hoechst 33342 (diluted 100 times with PBS) for 10 min, washed three times with PBS for 3 min each, and photographed under a microscope.

2.14. Co-staining of integrin α_3 and HSP60 experiment

The 4T1 cells were seeded in 96-well plates (1×10^4 cells/well) overnight and cells were treated with 40 μg/mL of AuNRs or AuNR-P17 for 24 h, then next, irradiated with or without a laser of 2.0 W/cm^2 for 2 min. The cells were fixed with −20 °C methanol at room temperature for 10 min, washed with PBS for three times. After adding 0.2 % Triton X-100 (diluted in PBS) for 5 min, the cells were washed with PBS for three times. The cells were blocked with blocking solution (1 % BSA-PBS) at room temperature for 1 h. The primary antibodies (Integrin Alpha 3 Polyclonal antibody and CoraLite®594-conjugated HSP60 Monoclonal antibody) were incubated at 4 °C overnight, and then washed with PBS for three times. The secondary antibodies (CoraLite®488-Conjugated AffiniPure Goat Anti-Rabbit IgG) were incubated for 1.5 h, and then washed with PBS for 3 times. The nuclei were stained with Hoechst (1:100) for 10 min, and then washed with PBS for 3 times. Finally, the cells were observed and photographed using a confocal microscope.

2.15. Mitochondrial function detection

The mitochondrial function indicators including mitochondrial membrane potential, intracellular ROS, and ATP levels were investigated. 4T1 cells were seeded in 96-well plates at a density of 1×10^4 cells per well and treated with nanorods at 40.0 μg/mL for 24 h. The cells were then washed with PBS and exposed to an 808-nm laser for 2.0 min at a power density of 2.0 W/cm^2. After a further 4 h of incubation, the cells were stained with JC-1 dye and 10 μM DCFH-DA for 30 min. The cells were then washed with PBS three times and observed under the fluorescence microscope. To measure intracellular ROS levels, cells were

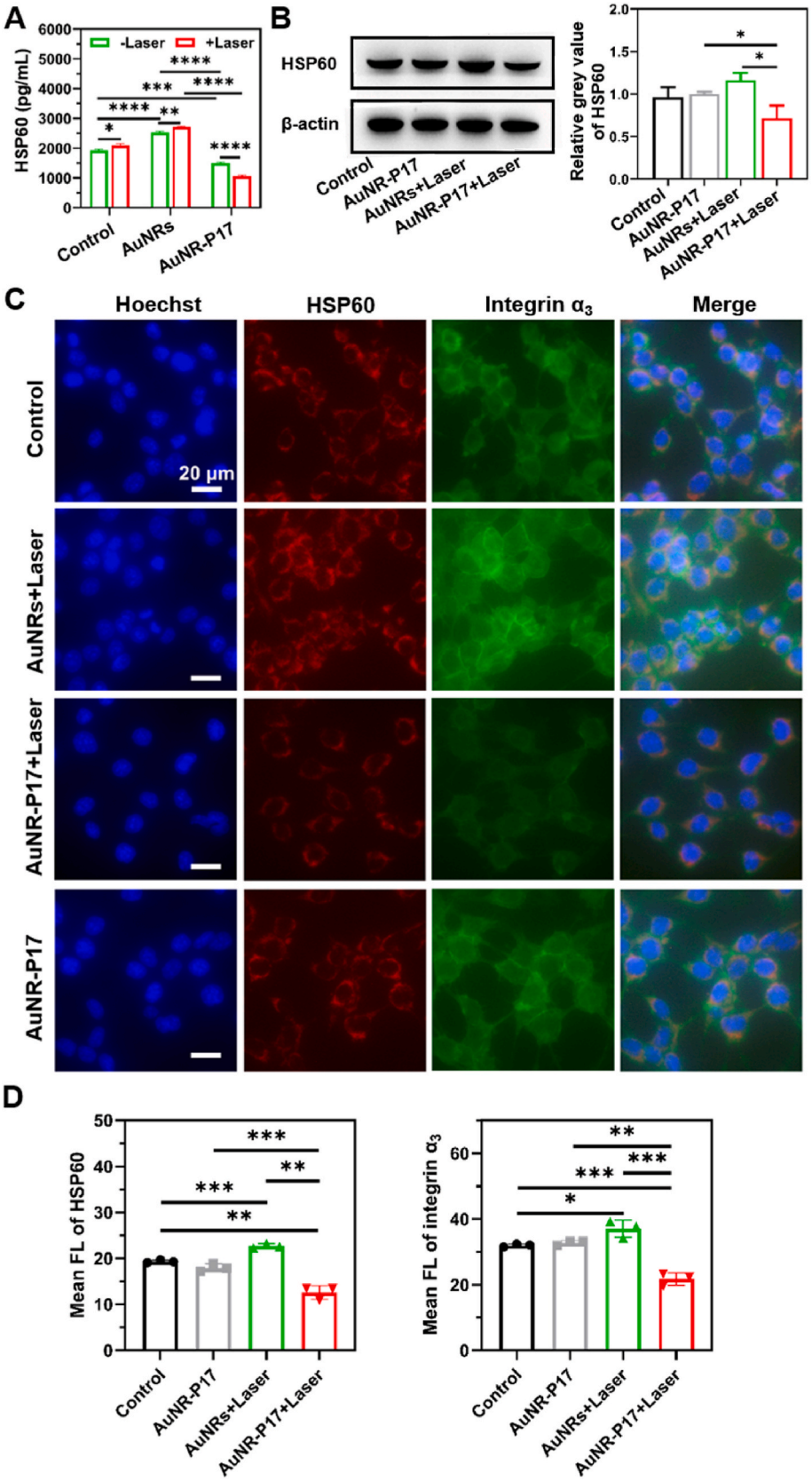

Fig. 3. AuNR-P17+Laser inhibited the expression of HSP60 and integrin α_3. (A) Total HSP60 levels of 4T1 cells with different treatments measured by ELISA assay. (B) Western blotting results of total HSP60 levels in 4T1 cells with different treatments. (C) Confocal images of 4T1 cells treated with AuNR-P17+Laser (2.0 W/cm^2). Nuclei stained with DAPI (blue), integrin α_3 stained with integrin α_3 antibody (green) and HSP60 stained with HSP60 antibody (red). The concentration of nanorods were 40 μg/mL and irradiation laser for 2 min (2.0 W/cm^2). Scale bar: 20 μm. (D) Statistical analysis for the fluorescence intensity of integrin α_3 and HSP60 in (C).

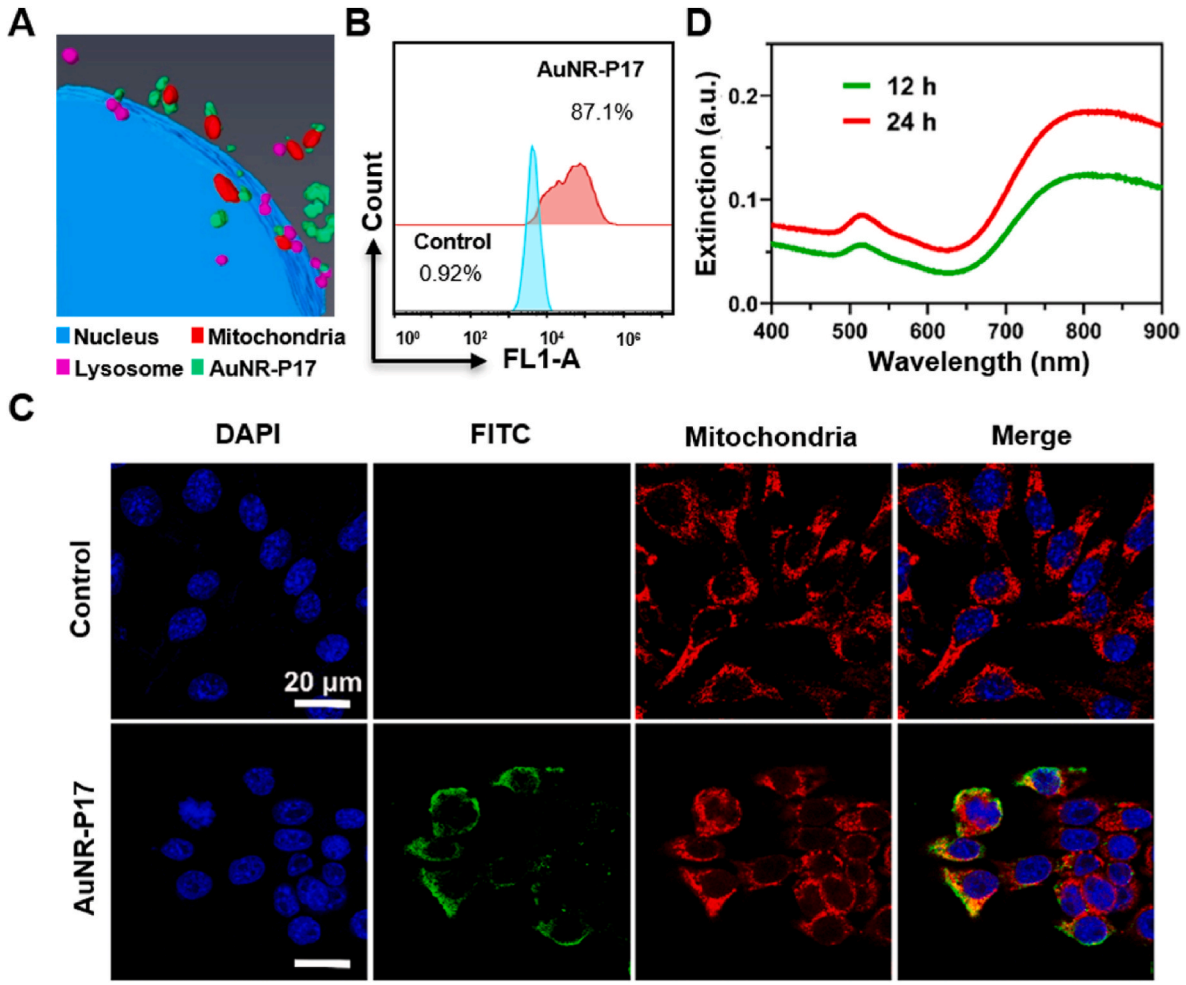

Fig. 4. Mitochondrial enrichment of AuNR-P17. (A) Localization of AuNR-P17 in 4T1 cells investigated with 3D nano-CT imaging. (B) Binding of AuNR-P17 (40 μg/mL) to 4T1 cells after 24 h incubation measured by flow cytometry. (C) Confocal microscopy images of AuNR-P17 (green) in cells after 24 h incubation. Nuclei stained with DAPI (blue), mitochondria stained with mitotracker Red CMXRos (red). Scale bar was 20 μm. (D) UV–vis–NIR extinction spectra of AuNR-P17 in mitochondria of 4T1 cells after 12 h or 24 h incubation.

collected and subjected to flow cytometry to estimate green fluorescence. Intracellular ATP levels were measured using an ATP assay kit following the same treatment regimen as described above.

2.16. Western blot analysis

To investigate the expression of anti-apoptotic and pro-apoptotic proteins (HSP60, p53, BCL-2, and Cleaved caspase-3) in 4T1 cells treated with nanorods at 40 μg/mL for 24 h, then irradiated with or without a laser of 2.0 W/cm^2 for 2 min, Western blot analysis was performed. Cells were cultured in RPMI medium, treated for 24 h, and irradiated. Cell lysates were prepared in RIPA lysis buffer, centrifuged, and loaded onto a gel. Proteins were separated, transferred to a PVDF membrane, and blocked with skim milk. Primary and secondary antibodies were incubated, and the membrane was developed using an enhanced chemiluminescence system.

2.17. DAMPs detection assay

In order to detect the extracellular release of DAMPs, 4T1 cells were seeded in 96-well plates at a density of 1×10^4 cells per well and treated with nanorods (40.0 μg/mL) for 24 h. Following treatment with or without an 808-nm laser for 1.5 min (2.0 W/cm^2) and incubation for 4 h, cells were collected, incubated with anti-CRT primary antibody for 30 min at 4 °C, washed with PBS, and subsequently incubated with an Alexa Fluor 647-conjugated secondary antibody for 30 min for flow cytometry analysis. 4T1 cells were also treated with nanorods and exposed to the 808-nm laser for 2.0 min (2.0 W/cm^2). Incubation with another 4 h, the cell supernatants were subjected to HSP60, HMGB1 ELISA Kit and ATP Determination Kits. DC 2.4 cells were cultured in 24-well plates at a density of 1×10^5 cells per well. The supernatant samples collected from the above DAMPs detection were added to DC 2.4 cells (300 μL of supernatant per well) and cultured for 24 h. Flow cytometry was employed to quantify the average fluorescence intensity of CD86 and MHCII on the cell surface of each group.

2.18. Tumor model and animal survival experiments

Female BALB/c mice, aged 6 weeks, were housed under specific pathogen-free conditions for 7 days at the Experimental Animal Center of the Institute of Basic Medical Sciences, Chinese Academy of Medical Sciences (Beijing, China) before tumor cell injection. Tumor-bearing mice were established by injecting 5×10^5 4T1 cells into the left fourth mammary fat pad. Once the tumor volume reached 125–200 mm^3 (on day 7 post-inoculation), the mice were randomly divided into six groups (n = 10 per group) and administered an intravenous injection of 5 % glucose (Control and Control + Laser group, 100 μL per mouse) or AuNRs/AuNR-P17 in 5 % glucose (1.25 mg/kg, 100 μL per mouse). The tumor sites were then irradiated with an 808-nm laser at 2.0 W/cm^2 for 3 min, between 12 and 24 h after the injection. The body weights of mice

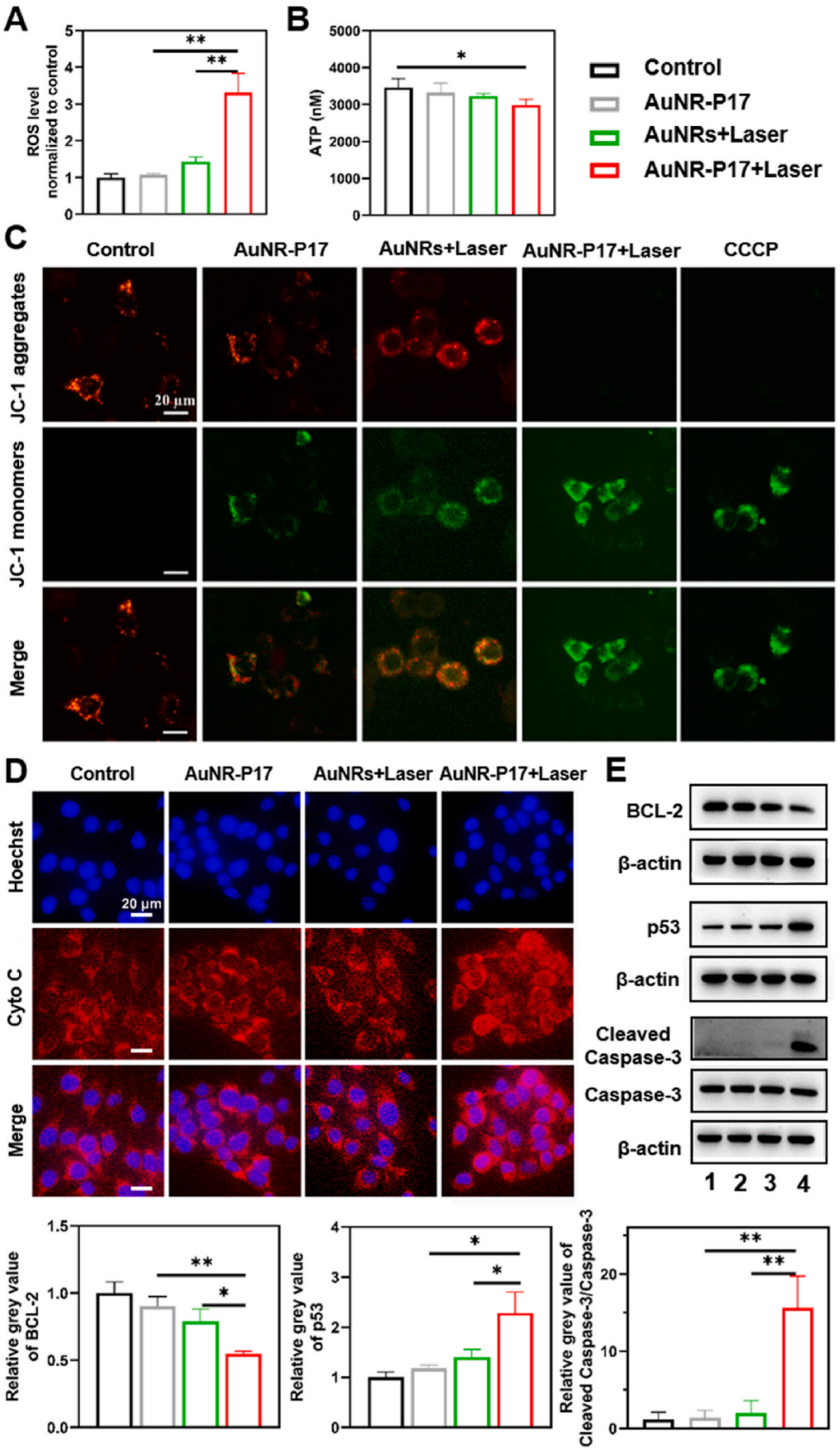

(caption on next page)

Fig. 5. Mitochondrial apoptosis induced by AuNR-P17+Laser. (A) cellular ROS and (B) total ATP of 4T1 cells treated with AuNRs and AuNR-P17 in the presence or absence of laser irradiation. (C) Confocal images of 4T1 cells with JC-1 staining, CCCP was used as positive control. (D) Confocal images of nucleus (blue) and Cyto C (red) of 4T1 cells. (E) Western blotting and the corresponding statistic results of BCL-2, p53 and Cleaved caspase-3 of 4T1 cells with different treatments. Numbers 1–4 refer to the Control, AuNR-P17, AuNRs + Laser and AuNR-P17+Laser (n = 3). The concentration of nanorods was 40 μg/mL and irradiation laser for 2 min (2.0 W/cm^2). Scale bar in (C) and (D) was 20 μm.

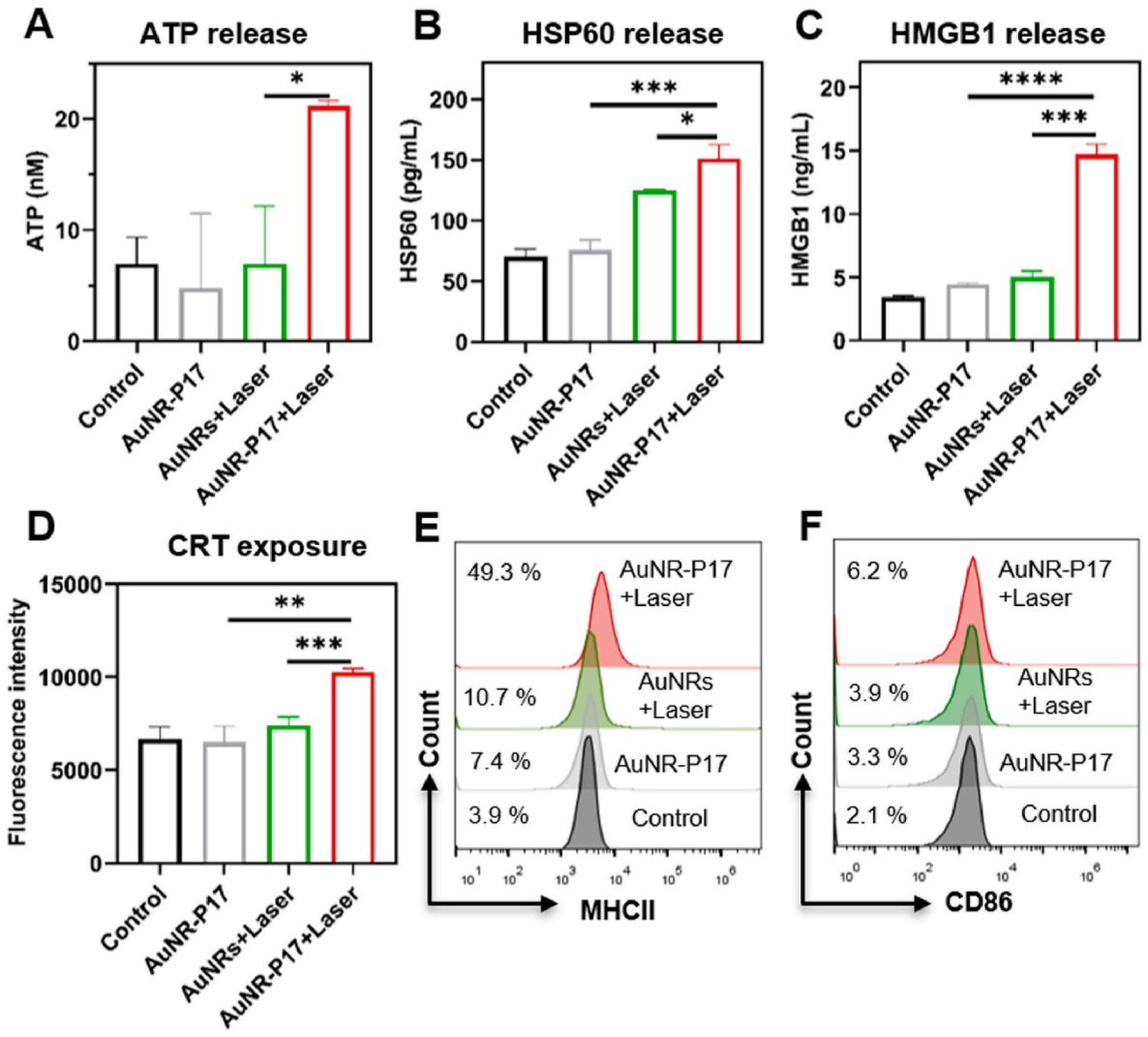

Fig. 6. Activation effects of DAMPs of 4T1 cells treated differently on DCs. The amounts of (A) ATP, (B) HSP60, and (C) HMGB1 released by the 4T1 cells quantified by ELISA, and (D) exposed CRT on the 4T1 cell membrane detected by flow cytometry. (E) and (F): Mean fluorescence intensity of MHCII and CD86 for the DC2.4 cells co-incubated with the supernatant of 4T1 cell treated differently, respectively (n = 3).

and tumor sizes were measured every two days, and the experimental endpoint was defined as death when tumor size exceeded 1500 mm^3.

2.19. Anti-tumor efficacy in vivo

The breast cancer xenograft 4T1 tumor model was established following the aforementioned protocol. At day 7 post-inoculation, the mice were randomly divided into four groups (n = 4 per group) and intravenously injected with AuNRs/AuNR-P17 in 5 % glucose at a dose of 1.25 mg/kg (100 μL per mouse). Between 12 and 24 h after injection, the tumor sites were subjected to 808-nm laser irradiation at 2.0 W/cm^2 for 3 min. The mice were monitored for changes in body weight and tumor size every 2 days. At day 21 post-inoculation, the mice were sacrificed and their livers, lungs, and tumor tissues were harvested and fixed in 4 % paraformaldehyde.

To detect DC maturation, mice were sacrificed at 72 h post-irradiation, and the maturation status of DCs from the tumor-draining lymph nodes was analyzed using flow cytometry. CD11c, CD80, and CD86 were co-stained with FITC, PE, and APC conjugates, respectively. Meanwhile, intratumoral CD8$^+$T cell infiltration was assessed by immunofluorescence staining of the harvested tumors. Additionally, the levels of tumor necrosis TNF-α and IFN-γ were measured using ELISA kits. Finally, the ROS levels in the tumor tissues were quantified using DCFH-DA solution.

2.20. H&E and immunofluorescence staining

The standard protocols provided by Servicebio (Wuhan, China) were employed for the execution of Hematoxylin and eosin (H&E), Ki67 staining and terminal deoxynucleotidyl transferase-mediated dUTP nick end labeling (TUNEL) as well as other immunofluorescence staining. The livers and lungs were fixed in 4 % paraformaldehyde and subjected

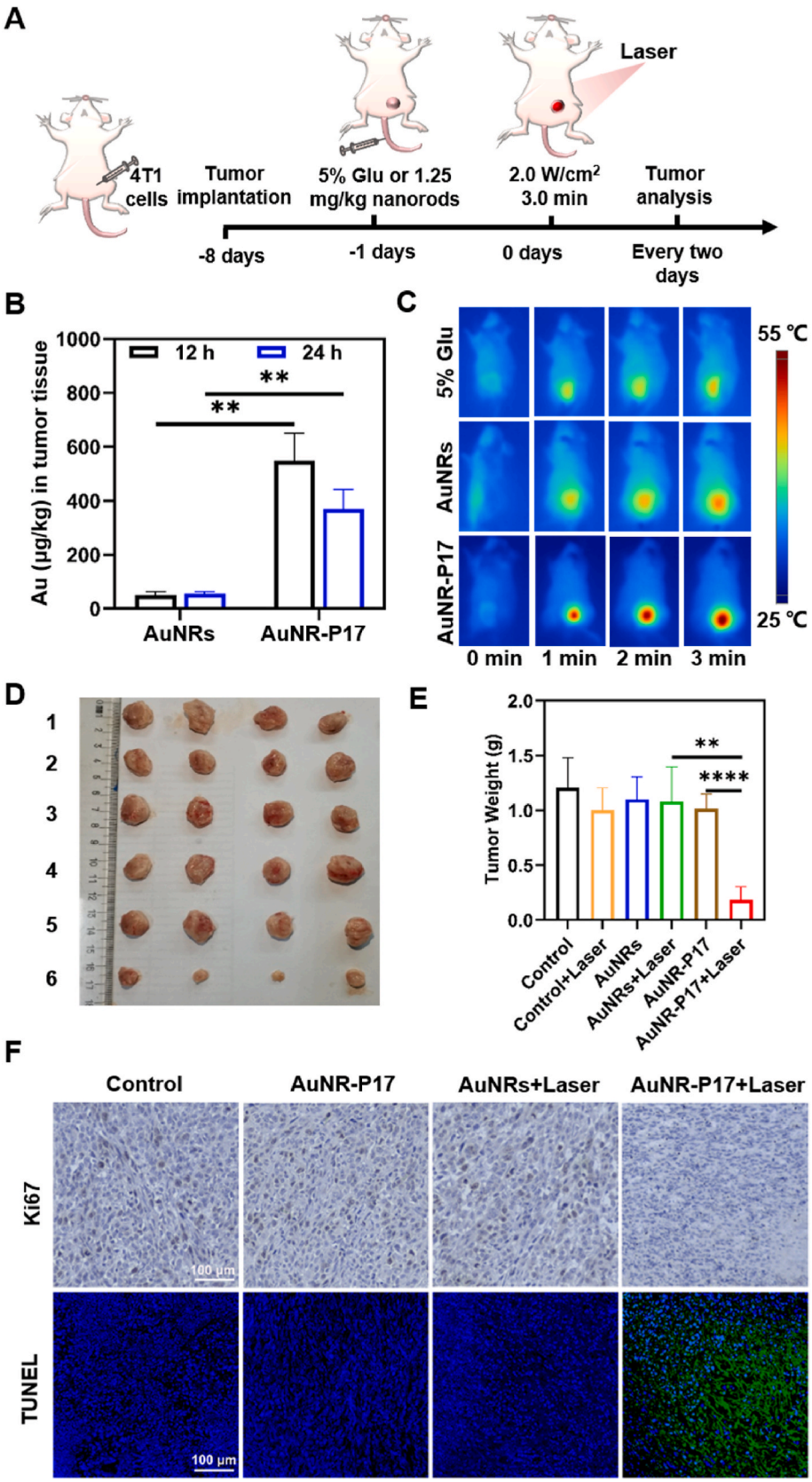

Fig. 7. Photothermal therapeutic effects of AuNR-P17 on TNBC mice. (A) Schematic diagram for the establishment and treatment of mouse model. (B) The concentration of gold in tumor tissues of mice for different periods post receiving AuNR-P17 measured by inductively coupled plasma mass spectrometry (ICP-MS) (n = 3). (C) Representative *in vivo* infrared thermal images of TNBC mice under laser irradiation after 24 h of intravenous injection. (D) Photos of the tumors in each group on 14th day after irradiation. Numbers 1–6 refer to the Control, Control + Laser, AuNRs, AuNRs + Laser, AuNR-P17 and AuNR-P17+Laser. (E) Tumor weight of mice received different treatments (n = 4). (F) Images of H&E for Ki67 antigen staining, and fluorescence TUNEL antigen (green) staining of tumor tissues. The scale bar was 100 μm.

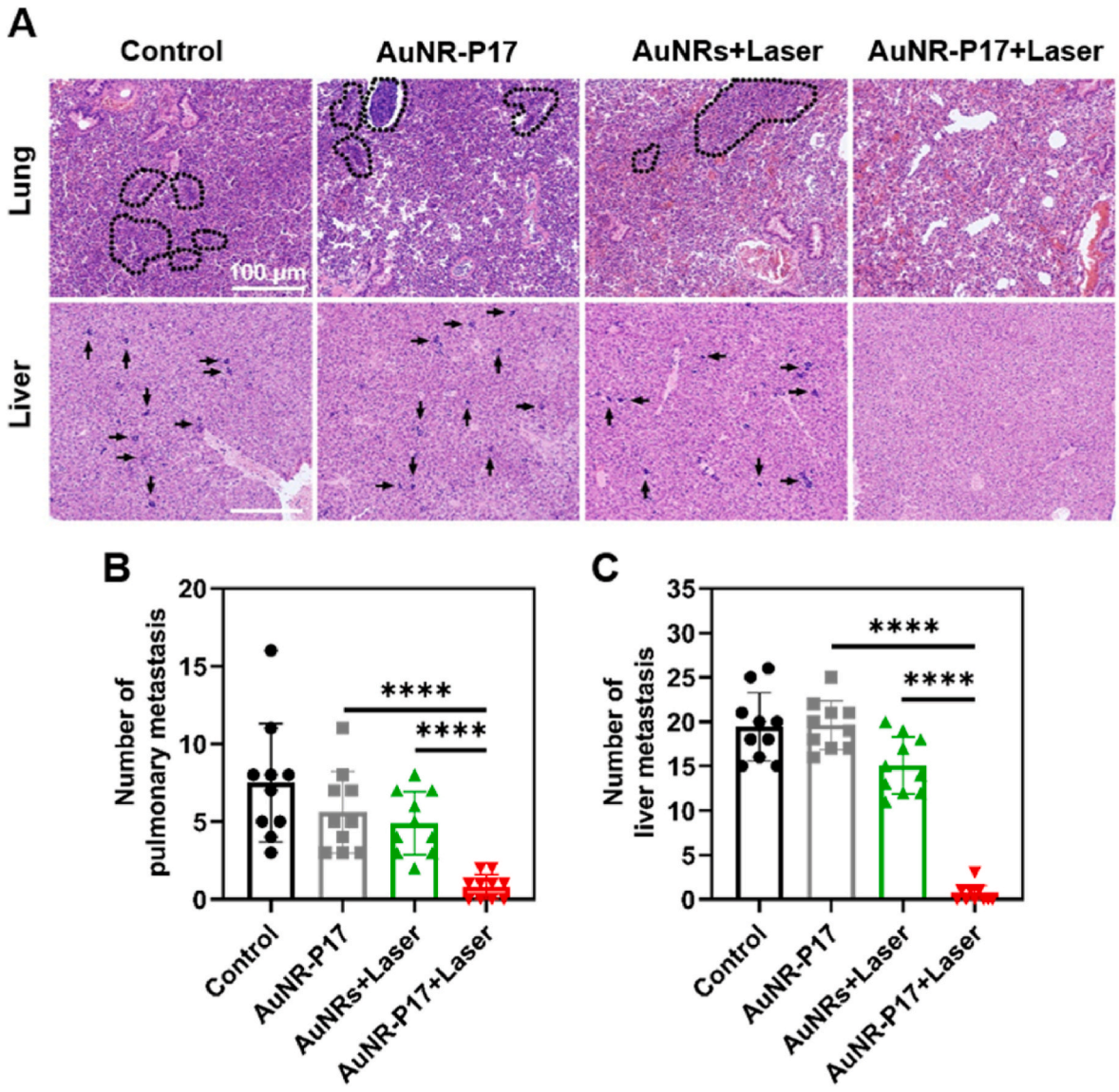

Fig. 8. Inhibitory effects of AuNR-P17+Laser on metastasis in the liver and lung of TNBC. (A) H&E staining images for lung and liver of mice in different groups. The dotted lines and arrows pointed metastatic nodules. Scale bar: 100 μm. Statistical results of metastatic nodules in (B) lung and (C) liver for 10 randomly selected different fields of view.

to H&E staining. For immunofluorescence staining, antibody (CD4, CD8, CD80, CD206, F4/80, Foxp3 and HSP60) was used and incubated at 4 °C overnight, followed by incubation with fluorescent secondary antibodies at room temperature for 1 h. Subsequently, the tumors were stained with a DAPI solution and imaged using an automatic multispectral imaging system (PerkinElmer).

2.21. ICP-MS

Triple negative breast cancer model was established and mice injected with nanorods. 20 μL of tail vein blood was collected from each mouse at 0, 1, 4, 12 and 24 h after injection. The mice were sacrificed at 12 or 24 h after injection, and the heart, liver, spleen, lung and tumor tissues of the mice were stripped. ICP-MS was used to detect Au content in blood, tissues and organs (n = 3).

2.22. Tumor-challenge and distant-tumor model

To further investigate the immunological memory induced in cured mice, on the sixth day after complete tumor ablation, 5×10^5 4T1 cells were inoculated into the right fourth mammary fat pad of mice in the AuNR-P17+Laser group (n = 3). The control group consisted of healthy mice that were inoculated with the same number of cells into the right fourth mammary fat pad (n = 3). The tumor volume of the mice was measured every two days.

In an effort to challenge conventional PTT strategies, we implemented a dual-tumor model in this study. Balb/c mice were subcutaneously inoculated with 5×10^5 4T1 cells in the left flank. After 7 days, the mice were subsequently inoculated with 5×10^5 4T1 cells in the right flank. On day −1, the mice were intravenously injected with AuNR-P17 at a dose of 1.25 mg/kg (100 μL per mouse). On day 0, the tumor sites on the left were treated with an 808-nm laser at 2.0 W/cm^2 for 3 min, resulting in complete tumor ablation. The sizes of the right tumors were then monitored every two days.

2.23. Cytotoxic immunological assay

To confirm the induction of specific immunological memory to TNBC cells in mice treated with AuNR-P17+Laser, mice with completely ablated tumors in the treatment group (n = 3) were sacrificed and their

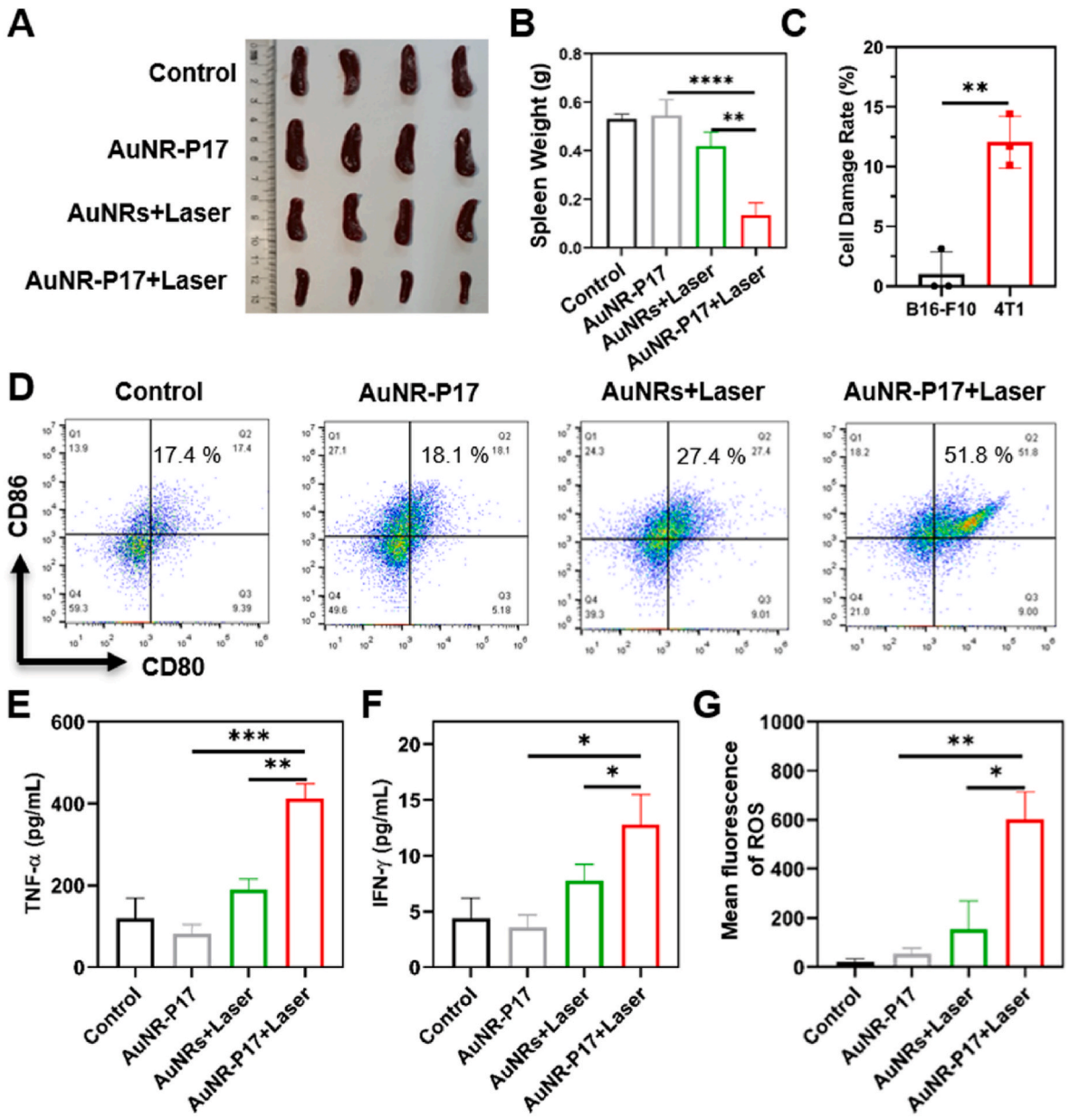

Fig. 9. AuNR-P17+Laser induced specific immune responses through ICD *in vivo*. (A) the photos and (B) weights of mice spleen in each group at 14th day after laser irradiation (n = 4). (C) Cell damage rate for the specific lymphocyte killing assay (n = 3). (D) Expressions of CD80 and CD86 for dendritic cells maturation in TLNs (gated on $CD11c^{+}$ dendritic cells) measured by flow cytometry (n = 4). (E) TNF-α and (F) IFN-γ in tumor tissue quantified by ELISA. (G) ROS levels in tumor tissue determined by DCFH-DA staining (n = 4).

spleens were harvested. Splenic lymphocytes, which served as effector cells, were isolated using a mouse splenic lymphocyte isolation kit. The effector cells were incubated with 4T1 or B16-F10 cells, which were used as target cells, for 4 h (the ratio of effector cells to target cells was 10:1). The damage rate of the cells was then detected using an LDH detection kit.

2.24. Safety assessment in vivo

In vivo safety assessment was conducted by administering 1.25 mg/kg of AuNRs/AuNR-P17 to healthy Balb/c mice via tail vein injection. On day 14, ocular blood samples were collected, and the mice were dissected to obtain their heart, liver, spleen, kidney, and lungs. The heart, liver, spleen, kidney, and lung specimens were fixed in 4 % paraformaldehyde and stained with hematoxylin and eosin (H&E). The blood samples were allowed to stand at room temperature for 3 h, after which they were centrifuged at 1000 rpm for 10 min. The resultant serum was transferred to fresh centrifuge tube and subjected to biochemical analysis using an automated biochemical analyzer to evaluate various parameters.

2.25. Statistical analysis

All results are expressed as mean ± standard error (SD) and the statistical significance of differences among them was determined by One-way analysis of variance (ANOVA). The survival curves were compared by the log-rank test using the Kaplan–Meier method. P-value less than 0.05 was considered statistically significant (*$p < 0.05$, **$p < 0.01$, ***$p < 0.001$ and ****$p < 0.0001$).

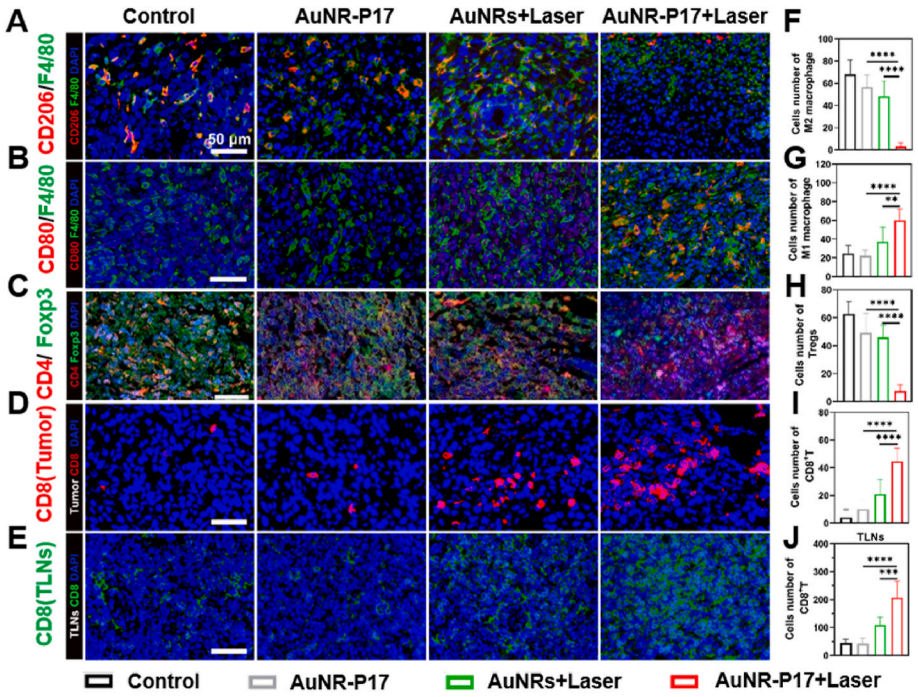

Fig. 10. Modulatory effects of AuNR-P17+Laser on the tumor microenvironment of TNBC mice. (A–E) Representative immunohistochemistry (IHC) and (F–J) corresponding statics analysis. (A, F) $CD206^{+}F4/80^{+}$ M2 macrophages, (B, G) $CD80^{+}F4/80^{+}$ M1 macrophages, and (C, H) $CD4^{+}Foxp3^{+}$ Tregs in the tumor. The $CD8^{+}$ T cells in the (D, I) tumor tissue and (E, J) TLNs. Scale bar: 50 μm. (F, G, H and I) Counts of the immune cells in the tumor tissues and (J) $CD8^{+}$ T cells in the TLNs of each group under 40 × magnification for 10 randomly selected different fields of view.

3. Results

3.1. Fabrication and characterizations of the conjugate of gold nanorods and P17

The conjugate of PSS coated gold nanorods and peptide 17 (AuNR-P17) was fabricated by one step reaction (Fig. 1A), remaining the rod-shape (Fig. 1B) and the longitudinal surface plasmon resonance (SPR) at 748 nm (Fig. 1C) of AuNR-P17, though exhibiting a red-shift in reference to 726 nm for AuNRs. The conjugate displayed negative charge on the surface, evidenced by the Zeta potential of −29.0 mV (Fig. 1D), the positive charges of P17 neutralized a part of the negative charge of AuNRs with −45.5 mV. The formation of the conjugate could be supported by other evidences including the Fourier transform infrared spectra (FT-IR) pattern of AuNR-P17 derived from AuNRs and P17 (Fig. 1E) and the characteristic peaks of Au and sulfur (S) shifted comparing with AuNRs or P17 in X-ray photoelectron spectroscopy (XPS) spectra (Figs. S1A and S1B). In addition, an obvious fluorescence peak appeared at 525 nm for AuNR-P17 was observed attributing to the presence of FITC on the peptide of P17 (Fig. S1C). Noted that AuNR-P17 had excellent stability in ddH_2O, 5 % glucose and cell culture medium, neither Zeta potential nor particle size changed over time (Figs. S1D, S1E, S1F and S1G). The cytotoxicity of AuNRs and AuNR-P17 on breast cancer tumor cell line 4T1 was firstly examined using CCK-8 assay. The cells were incubated with AuNR-P17 at different concentrations, and AuNRs were taken as controls. It was shown that AuNRs and AuNR-P17 both showed little cytotoxicity when the concentrations of AuNRs were no more than 40 μg/mL, the relative viabilities of the cells were higher than 80 % (Fig. 1F).

3.2. AuNR-P17 elicited much stronger photothermal effects in vitro

As consistent with literature, it was detected that HSP60 was highly expressed both on the membrane and in the cytoplasm of 4T1 cells (Fig. S2). First of all, PTT effects of the different nanorods on 4T1 cells were investigated. Observed from the extinction spectra of the cells incubated with AuNRs and AuNR-P17, it was seen that the intensity of the characteristic extinction of AuNR-P17 was higher than that of AuNRs (Fig. 2A), suggesting that more AuNRs entered into the cells by the aid of P17 [27]. The irradiation of 808 nm laser following 24 h incubation of nanorods at 40 μg/mL resulted in sharp increase of temperature for the solution. It was shown that the temperature of AuNRs group was increased to 38 °C and 44 °C responsible for the irradiation time of 1 min and 2 min, respectively, and the temperature of AuNR-P17 group was increased to 42 °C and 51 °C for the two irradiation periods, respectively (Fig. 2B). The significant difference between the temperatures led to the significant difference of the relative cell viability: with irradiation of 2 min, the cell viability of AuNR-P17 group was decreased to 2.8 %, while that of AuNRs group was 47.8 % (Fig. 2C). Therefore, the approach of laser irradiation following AuNR-P17 incubation (named as AuNR-P17+Laser) exhibited a remarkably and much stronger effective tumor-killing capacity than AuNRs + Laser, with almost complete tumor cell destruction. As shown in Fig. 2D, a larger amount of dying cells showed yellow fluorescence that was merged by red for dying cell and green of FITC-labeled P17, providing further evidence that AuNR-P17+Laser induced remarkable cell death than AuNRs + Laser, because much more AuNR-P17 entered into the cells than AuNRs.

3.3. AuNR-P17 down-regulated HSP60 level and enriched in mitochondrial

It has been recognized that the HSP60 level up-regulates when cells are under heat stimulation, which reduces the efficacy of PTT [28,29]. Therefore, we examined whether AuNR-P17 affected the level of HSP60 by ELISA assay and western blotting. Results showed that HSP60 in the cell lysate was decreased when the cells were irradiated following AuNR-P17 incubation (Fig. 3A), on the contrary, the HSP60 level of AuNRs + Laser group significantly increased to response the heat stimulation. Results obtained from the western blotting (Fig. 3B) were consistent with that of ELISA assay. Besides, it could be noticed that

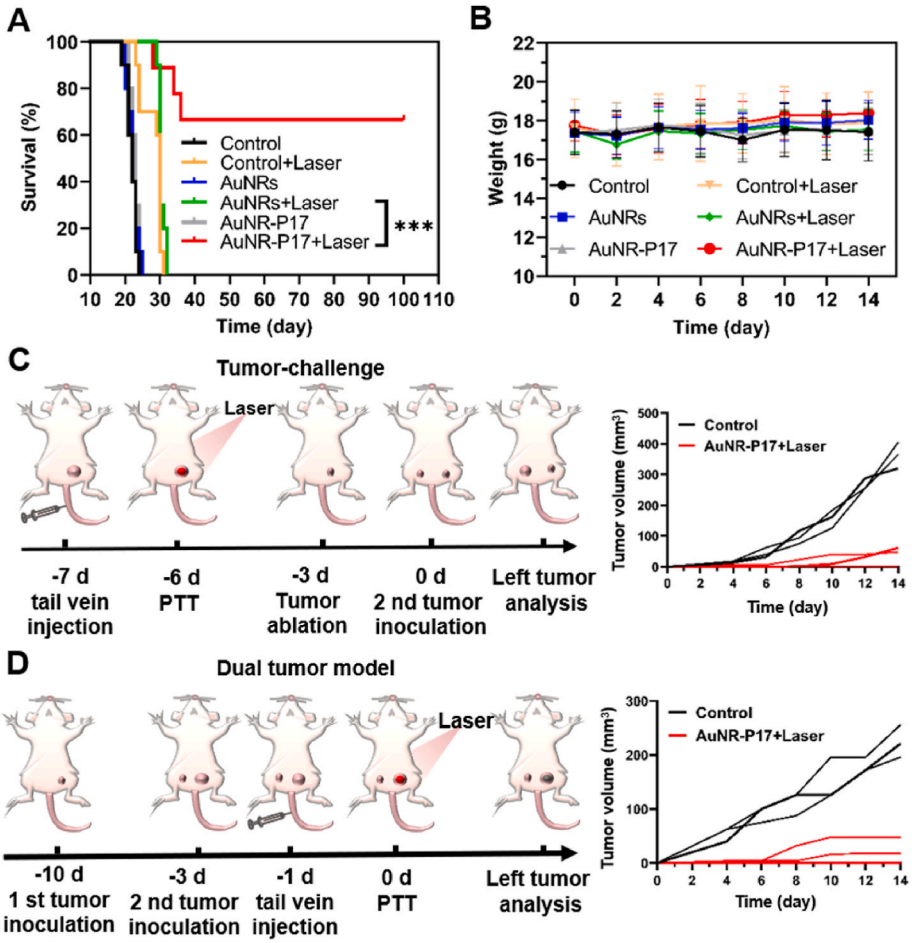

Fig. 11. Specific and longer immunological memory against tumor induced by AuNR-P17+Laser. (A) Survival curves of mice received different treatments (n = 10). (B) Body weights after different treatments (n = 10). (C) Treatment regime for tumor challenge and the tumor volume for challenge experiment (n = 3). (D) Treatment regime for dual tumor model and the tumor volume for the dual-tumor experiment (n = 3).

AuNR-P17 alone was able to reduce the level of HSP60 even without the laser irradiation. These results together indicated that P17 significantly weakened the heat stress of the cells. In addition, results from the confocal microscopy (Fig. 3C) and statistical analysis (Fig. 3D) showed that AuNR-P17+Laser significantly down-regulated the level of integrin α_3 along with the decrease of HSP60, suggesting AuNR-P17 interfered the combination of the two proteins. It is documented that HSP60 on cell membrane can interact with integrin $\alpha_3\beta_1$ to continuously promote tumor metastasis [30,31], therefore, our results indicated that AuNR-P17+Laser was beneficial for enhancing thermal sensitivity of the tumor cells and inhibiting tumor migration mediated by HSP60.

Synchrotron radiation-based soft X-ray nanocomputed tomography (nano-CT) revealed that a lot of AuNR-P17 co-located with mitochondria and cytoplasm of the cells, with a small part in the lysosomes (Fig. 4A) according to the differences in the absorption of X-ray photons by elements and the three-dimensional morphological characteristics of the organelle [32–35]. Results obtained from flow cytometry showed that AuNR-P17 was of highly affinity to the cells with a binding rate of 87.1 % (Fig. 4B), and observations from confocal microscopy showed that AuNR-P17 (green) could be co-located with mitochondria (red) after incubated for 24 h (Fig. 4C). Moreover, extracted mitochondria from the cells incubated with AuNR-P17 displayed the characteristic extinction spectrum of AuNR-P17, and the peak intensity increased with the incubation time (Fig. 4D). These results collectively indicated that AuNR-P17 enriched in mitochondria of the tumor cells. Images of TEM presented supporting evidence that AuNR-P17 located at mitochondria and cytoplasm, while AuNRs mainly distributed in the lysosomes (Fig. S3).

3.4. Mitochondrial apoptosis induced by AuNR-P17+Laser

It was shown that the cellular reactive oxygen species (ROS) was increased and the cellular ATP decreased when treated with AuNR-P17+Laser (Fig. 5A and B), indicating the occurrence of mitochondrial damage. Therefore, we examined whether the apoptosis underwent via the mitochondrial pathway. Herein, fluorescence staining of JC-1 was used to evaluate the mitochondrial membrane potential of 4T1 cells. As shown in Fig. 5C, AuNR-P17+Laser significantly reduced mitochondrial membrane potential, similar to that induced by the mitochondrial electron transport chain inhibitor carbonyl cyanide m-chlorophenylhydrazone (CCCP). In addition, the cytosol release of Cyto C was examined to figure out whether caspase cascades of apoptosis was activated [36]. As shown in Fig. 5D, the Cyto C was increased when cells were treated with AuNR-P17+Laser. Furthermore, results of western blotting showed that the level of anti-apoptotic protein BCL-2 was down-regulated, and pro-apoptotic protein p53 and cleaved caspase-3 protein were significantly up-regulated in the cells treated with AuNR-P17+Laser (Fig. 5E), indicating that AuNR-P17+Laser induced mitochondrial apoptosis effectively in the tumor cells.

3.5. AuNR-P17+Laser induced effective ICD in vitro

It is well documented that mitochondrial apoptosis can induced ICD [37,38]. Next, we tried to figure out whether effective ICD was triggered

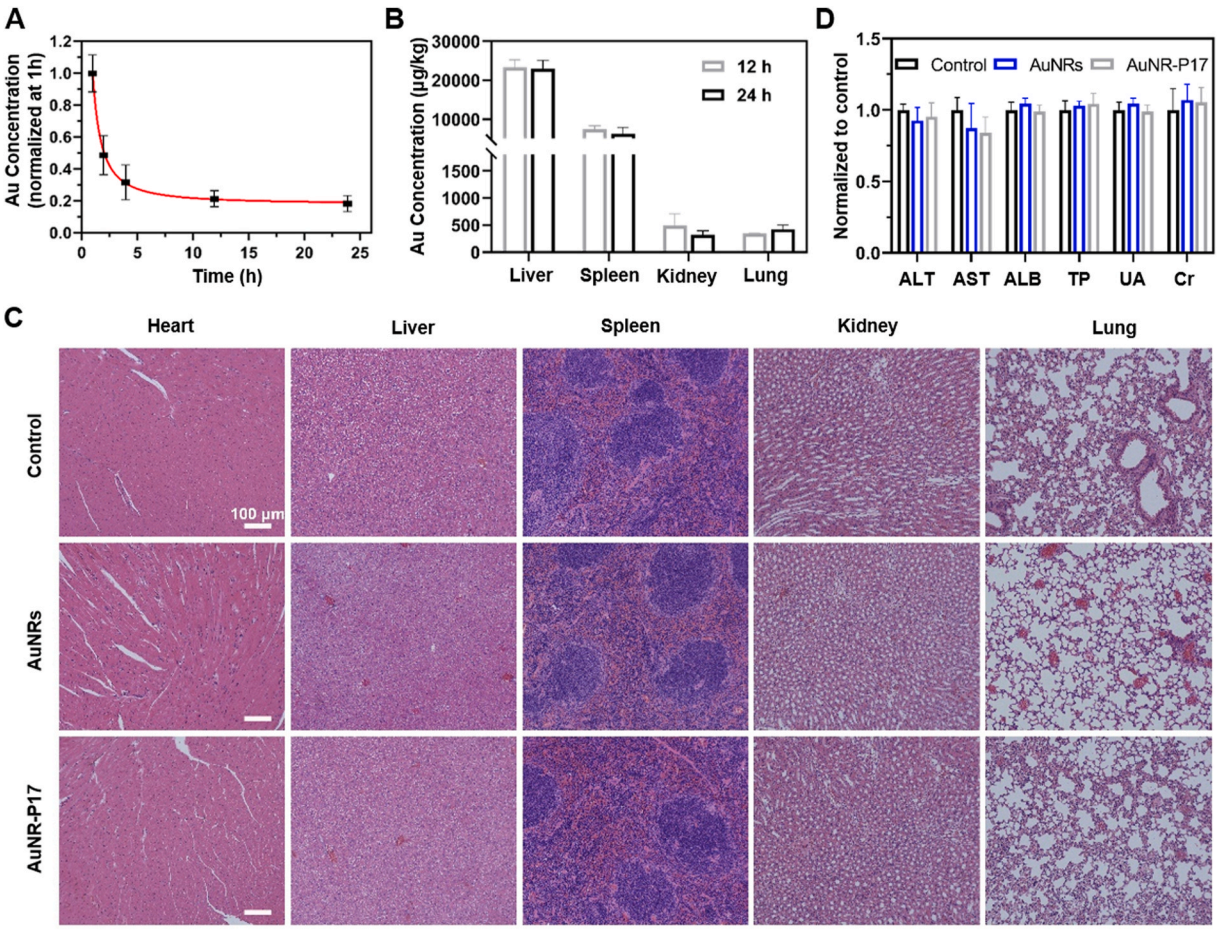

Fig. 12. Safety assessment on AuNRs and AuNR-P17 *in vivo*. (A) Au concentration in blood circulation at different time. (B) Biodistribution of Au in different organs after treated for 12 h and 24 h. (C) The histopathological changes in different organs with H&E staining after 14 days of the injections. (D) Changes of biochemical parameters in liver and kidney function after 14 days of the injections. The scale bar was 100 μm and n = 3 for all the safety assessment experiments.

by examining the amounts of DAMPs including CRT exposure and HMGB1 release, HSP60 and ATP of 4T1 cells treated differently. It was shown that the amounts of ATP, HSP60 and HMGB1 in the supernatants (Fig. 6A–C) and CRT exposure on the cell membrane (Fig. 6D) in the group of AuNR-P17+Laser were the highest ones among all the tested groups, and it could be noticed that AuNRs + Laser was not able to increase the amounts of CRT exposure and release of HMGB1, HSP60 and ATP, which clearly indicated the importance of cellular organelle location for AuNRs as a photothermal agent. These DAMPs effectively activated dendritic cells (DCs) DC2.4, evidenced by the upregulations of maturation markers MHCII and CD86. As shown that the mean fluorescence intensities of MHCII and CD86 for AuNR-P17+Laser group were the highest ones among all the tested groups, while AuNRs + Laser was not able to significantly induce the DCs to undergo maturation (Fig. 6E and F).

3.6. Photothermal therapeutic effects of AuNR-P17+Laser on TNBC mice

Next, the breast cancer xenograft 4T1 tumor model was established to explore the therapeutic potential of AuNR-P17+Laser. As shown in Fig. S2B, HSP60 was highly expressed in the tumor issues. The administration regimes were shown in Fig. 7A. First, the contents of gold in tumor tissues were examined at 12 h and 24 h post-injection. It was showed that for mice received AuNR-P17 they were 10.7 and 6.7 times that of mice received AuNRs, respectively (Fig. 7B), again exhibiting the active targeting role of P17. After irradiated for same time, the tumor temperatures of mice in AuNR-P17+Laser group were much higher than those in AuNRs + Laser group, evidenced by the observation of thermal images (Fig. 7C). Consequently, the tumor volume (Fig. 7D and S4) and weight (Fig. 7E) of mice in AuNR-P17+Laser group were significantly smaller and less than those of the other groups, respectively. On the 3rd day after laser irradiation, tumor tissues were stripped from the mice and stained with Ki67 and TUNEL, results showed that AuNR-P17+Laser strongly inhibited the cell proliferation and promoted apoptosis of the tumor cells (Fig. 7F). Importantly, on the 14th day post-irradiation, the number of tumor metastasis nodules in lung and liver of mice received AuNR-P17+Laser treatment (Fig. 8A) was significantly less than that of the other groups (Fig. 8B and C), showing the remarkable inhibitory effects of AuNR-P17+Laser on the liver and lung metastasis of TNBC.

3.7. AuNR-P17+Laser induced specific immune responses against tumor in vivo

One of the pathological features of the 4T1 tumor model is splenomegaly caused by granulocyte hyperplasia [39], and remission of splenomegaly is related to immune responses against the tumor [40]. In this study, on the 14th day after laser irradiation, the spleen weight of mice in AuNR-P17+Laser group was significantly less than that in the other groups (Fig. 9A and B), suggesting the treatment induced the strongest immune responses. Next, lymphocytes in the spleen of mice treated with the AuNR-P17+Laser were incubated with 4T1 and mouse melanoma cells B16-F10, results showed that the 4T1 cells were effectively killed by the lymphocytes while the B16-F10 cells were killed little (Fig. 9C), indicating that a specific immune response to 4T1 cells was generated in the mice. Moreover, mice received AuNR-P17+Laser treatment remarkably promoted dendritic cells maturation in the

tumor-draining lymph nodes (TLNs), evidenced by the significant increase of $CD80^+$ and $CD86^+$ (Fig. 9D). At the same time, levels of immune-related factors, including tumor necrosis factor-α (TNF-α) and interferon-γ (IFN-γ) were all elevated significantly (Fig. 9E and F), and the ROS level in the tumor tissue was increased as well (Fig. 9G). These results indicated that AuNR-P17+Laser induced strong and specific immune responses through ICD *in vivo*.

3.8. AuNR-P17+Laser modulated the tumor microenvironment to immunoreactive in vivo

It is widely accepted there are large amounts of M2 macrophages and regulatory T lymphocytes in the immunosuppressive tumor microenvironment, and infiltrations of $CD8^+$ T cells and M1 macrophages would change the immunosuppressive status to immunoactive one [41]. Therefore, we examined the status of tumor microenvironment in each group with immunofluorescent staining. It was shown that after treated with AuNR-P17+Laser, the number of $CD206^+F4/80^+$ M2 macrophages (Fig. 10A and F) and $CD4^+Foxp3^+$ Tregs (Fig. 10C and H) in the tumor tissue of mice decreased, while the number of $CD80^+F4/80^+$ M1 macrophages (Fig. 10B and G) in the tumor tissue increased. It should be noted that $CD8^+$ T cells significantly increased both in the tumor tissue (Fig. 10D and I) and in the TLNs (Fig. 10E and J), evidenced by a greater number of $CD8^+$T cells infiltrating. These results demonstrated that the strategy of AuNR-P17+Laser was highly effective in modulating the immunosuppressive tumor microenvironment to the immunoreactive one.

3.9. AuNR-P17+Laser induced specific and longer immunological memory against tumor in vivo

Animal experimental results showed that AuNR-P17+Laser significantly prolonged the survival time of mice compared to the other groups (Fig. 11A), the median survival time and overall survival time were both longer than 100 days, in comparison, the median and overall survival for control group was 22 days and 24 days respectively. Meanwhile, no significant effects on the body weight of mice were observed within 14 days after tail intravenous injection in all tested groups (Fig. 11B), suggesting all the treatments were safe *in vivo*. To verify the immunological memory response, mice treated with the AuNR-P17+Laser were contralateral inoculated with the same number of 4T1 cells for the tumor-challenge experiment [42], the inoculation day was recorded as day 0, and the Control group refers to the cells inoculated in the same side of healthy mice (Fig. 11C). Results showed that the contralateral tumor growth of mice that had been treated with AuNR-P17+Laser was effectively inhibited (Fig. 11C). In a dual-tumor model [43], when the primary tumor was irradiated with laser following intravenous injection of AuNR-P17, the distant tumor growth was inhibited as well (Fig. 11D), which further confirmed that AuNR-P17+Laser elicited specific and longer immunological memory in TNBC mice.

3.10. Safety assessment of gold nanorods in vivo

After injected via tail vein, the content of Au in the blood circulation and the biodistribution of Au in the primary tumor and organs were determined by using ICP-MS. For mice of AuNR-P17 group, Au content in the circulating blood decreased rapidly within 4 h and reached equilibrium within 24 h (Fig. 12A), and Au was mainly detected in the liver and spleen, while small amount existed in the kidney and lung (Fig. 12B). To further evaluate the safety of AuNRs and AuNR-P17, we examined hepatic and renal biochemical indicators as well as analyzed pathological morphology of heart, liver, spleen, lung and kidney with H&E staining on the 14th day after intravenous injection in healthy mice. The H&E staining images showed no apparent damage on the organ tissues after the treatments (Fig. 12C). In addition, the hepatic functional parameters of alanine aminotransferase (ALT), aspartate aminotransferase (AST), total serum protein (TP) and albumin (ALB), and the renal functional parameters of creatinine (Cr) and blood uric acid (UA) showed little changes (Fig. 12D).

4. Discussion

HSP60 is initially regarded as a mitochondrial chaperone protein that is crucial for protein folding, accumulating data support that it is localized in different compartments including cytosol, outer mitochondrial surface, cell surface, intracellular vesicles, nucleus, extracellular space, and even in blood circulation. Increased level of HSP60 has been detected from both solid tumor tissues including breast cancer and leukemia, and which is correlated with poorer prognosis [44]. HSP60 can regulate tumor cell function depending on its subcellular location. For example, HSP60 locating within the tumor cells is able to mediate heat tolerance and associated with cell apoptosis [9], while that on the cell membrane can combine with integrin $\alpha_3\beta_1$ to promote breast cancer cell metastasis [30].

In this study, HSP60 was taken as a promising target to direct the enrichment of AuNRs in mitochondria as well to overcome heat resistance of the TNBC tumor cells. The reasons are as follows. First, HSP60 is predominantly localized in mitochondria and overexpressed on the surface of TNBC cells, as evidenced in previous studies [21,22,24]. Second, HSP60 serves as a functional protein that facilitates tumor cell drug resistance and metastasis through heat tolerance [30,31,45]. It is well known that the expression of HSP60 increases when the cells suffer heat stress, subsequently diminishing the efficacy of PTT [29], for examples, HSP inhibitors can decrease the expression of HSP and enhance the thermal sensitive of tumor cells during PTT [10,11,29,46].

In our previous study, P17 was synthesized and demonstrated to be able to specifically bind to HSP60 in multiple tumor cells, and it was used to label apoptotic cells because a large amount of HSP60 entered cytoplasm from mitochondria when the cells underwent apoptosis [25]. In this work, we revealed P17 could also down regulate the level of HSP60 for the breast cancer tumor cells. Our results showed that, regardless of laser irradiation, AuNR-P17 down-regulated the HSP60 levels and inhibited the cells heat-stressful function. This is advantageous for enhancing the thermal sensitivity of tumor cells. Moreover, the decrease of HSP60 on the cell's membrane led to the blockade of the interaction between HSP60 and integrin α_3. Integrin $\alpha_3\beta_1$ is a cell adhesion receptor for certain laminins, which is known to promote breast tumor growth and invasion [47]. It has been reported that HSP60 on cell membrane can interact with integrin $\alpha_3\beta_1$ to promote tumor metastasis [30,31], therefore, the disruption of the interaction between HSP60 and integrin α_3 would be beneficial for inhibiting tumor migration.

Our experimental results also demonstrated that AuNR-P17 can effectively translocate to mitochondria by binding to membrane HSP60, which is an interesting pathway of one key opening two doors. Moreover, mitochondria-targeted PTT induced significant ICD of the tumor cells [48,49], evidenced in the immunological responses of AuNR-P17+Laser in Fig. 6, while AuNRs + Laser were not able to induce sufficient ICD without HSP60 targeting. These validated the importance of HSP60 as a dual-target, induction of mitochondrial-cell death and inhibition of heat stress. Concurrently, AuNR-P17 coupled with laser irradiation effectively induces mitochondrial apoptosis in tumor cells and triggers robust and long-lasting specific immune responses against TNBC. Searching novel and effective therapeutic targets for TNBC remains a challenge [50], and our results strongly suggest that HSP60 is a new promising therapeutic target for PTT-based treatment of TNBC.

5. Conclusions

In summary, a novel conjugate AuNR-P17 that precisely targets HSP60, a protein expressed on the membrane and stored in mitochondria of TNBC cells, was fabricated and characterized. The conjugate

holds dual functions including mitochondrial targeting and HSP60 downregulation. In this case, AuNR-P17+Laser triggered effective mitochondrial apoptosis in the tumor cells, eliciting robust and long-lasting specific immune responses against TNBC. Furthermore, the conjugate itself can impair HSP60's thermotolerance ability and blockade the interaction between HSP60 and integrin α_3. These effects collectively inhibit metastasis and relapse in the TNBC mice, significantly extending the animal's survival up to 100 days. This study not only identifies HSP60 as a promising new therapeutic target but also exhibits a promising modality of photothermal immune therapy to TNBC.

CRediT authorship contribution statement

Yiling Meng: Writing – original draft, Visualization, Methodology, Investigation. **Tao Wen:** Writing – review & editing, Supervision, Methodology, Investigation, Conceptualization. **Xuanxin Liu:** Methodology. **Aiyun Yang:** Methodology. **Jie Meng:** Methodology, Formal analysis. **Jian Liu:** Formal analysis. **Jianhua Wang:** Funding acquisition. **Haiyan Xu:** Writing – review & editing, Supervision, Funding acquisition, Conceptualization.

Declaration of competing interest

The authors declare that they have no known competing financial interests or personal relationships that could have appeared to influence the work reported in this paper.

Data availability

Data will be made available on request.

Acknowledgments

This work was supported by National Key R&D Program of China (no. 2022YFA1205803), the CAMS Innovation Fund for Medical Sciences (CIFMS) (no. 2021-1-I2M − 026), and the Research Foundation of Capital Institute of Pediatrics (JHYJ-2023-03). We thank Prof. Yong Guan (beamline BL07W of the National Synchrotron Radiation Laboratory, University of Science and Technology of China, Hefei, China) for his help on the nano-CT images and Prof. Lizeng Gao (Institute of Biophysics, Chinese Academy of Sciences, Beijing, China) for his help on TEM for cells.

Appendix A. Supplementary data

Supplementary data to this article can be found online at https://doi.org/10.1016/j.mtbio.2024.101282.

References

[1] WHO, Global cancer burden growing, amidst mounting need for services. https://www.who.int/news/item/01-02-2024-global-cancer-burden-growing-amidst-mounting-need-for-services, 2024 (accessed 1February 2024).
[2] N. Harbeck, M. Gnant, Breast cancer, Lancet 389 (2017) 1134–1150, https://doi.org/10.1016/s0140-6736(16)31891-8.
[3] F. Ye, S. Dewanjee, Y. Li, N.K. Jha, Z.S. Chen, A. Kumar, Vishakha, T. Behl, S. K. Jha, H. Tang, Advancements in clinical aspects of targeted therapy and immunotherapy in breast cancer, Mol. Cancer 22 (2023) 105, https://doi.org/10.1186/s12943-023-01805-y.
[4] C. Anders, L.A. Carey, Understanding and treating triple-negative breast cancer, Oncol. 22 (2008) 1233–1239.
[5] K.K. Thakur, D. Bordoloi, A.B. Kunnumakkara, Alarming burden of triple-negative breast cancer in India, Clin. Breast Cancer 18 (2018) e393–e399, https://doi.org/10.1016/j.clbc.2017.07.013.
[6] L. Yin, J.J. Duan, X.W. Bian, S.C. Yu, Triple-negative breast cancer molecular subtyping and treatment progress, Breast Cancer Res. 22 (2020) 61, https://doi.org/10.1186/s13058-020-01296-5.
[7] S.R. Kirchhoff, S. Gupta, A.A. Knowlton, Cytosolic heat shock protein 60, apoptosis, and myocardial injury, Circulation 105 (2002) 2899–2904, https://doi.org/10.1161/01.cir.0000019403.35847.23.
[8] Y.X. Shan, T.J. Liu, H.F. Su, A. Samsamshariat, R. Mestril, P.H. Wang, Hsp10 and Hsp60 modulate Bcl-2 family and mitochondria apoptosis signaling induced by doxorubicin in cardiac muscle cells, J. Mol. Cell. Cardiol. 35 (2003) 1135–1143, https://doi.org/10.1016/s0022-2828(03)00229-3.
[9] E. Song, S. Tang, J. Xu, B. Yin, E. Bao, J. Hartung, Lenti-siRNA Hsp60 promote bax in mitochondria and induces apoptosis during heat stress, Biochem. Biophys. Res. Commun. 481 (2016) 125–131, https://doi.org/10.1016/j.bbrc.2016.10.153.
[10] T.Y. Lin, W. Guo, Q. Long, A. Ma, Q. Liu, H. Zhang, Y. Huang, S. Chandrasekaran, C. Pan, K.S. Lam, Y. Li, HSP90 inhibitor encapsulated photo-theranostic nanoparticles for synergistic combination cancer therapy, Theranostics 6 (2016) 1324–1335, https://doi.org/10.7150/thno.14882.
[11] H.J. Liu, M. Wang, X. Hu, S. Shi, P. Xu, Enhanced photothermal therapy through the in situ activation of a temperature and redox dual-sensitive nanoreservoir of triptolide, Small 16 (2020) e2003398, https://doi.org/10.1002/smll.202003398.
[12] W. Tao, N. Wang, J. Ruan, X. Cheng, L. Fan, P. Zhang, C. Lu, Y. Hu, C. Che, D. Sun, J. Duan, M. Zhao, Enhanced ROS-boosted phototherapy against pancreatic cancer via nrf2-mediated stress-defense pathway suppression and ferroptosis induction, ACS Appl. Mater. Interfaces 14 (2022) 6404–6416, https://doi.org/10.1021/acsami.1c22861.
[13] E. Hwang, H.S. Jung, Organelle-targeted photothermal agents for cancer therapy, Chem. Commun. 57 (2021) 7731–7742, https://doi.org/10.1039/d1cc02168k.
[14] Y.H. Li, H.R. Jia, H.Y. Wang, X.W. Hua, Y.W. Bao, F.G. Wu, Mitochondrion, lysosome, and endoplasmic reticulum: which is the best target for phototherapy? J. Contr. Release 351 (2022) 692–702, https://doi.org/10.1016/j.jconrel.2022.09.037.
[15] S. Ganapathy-Kanniappan, Targeting tumor glycolysis by a mitotropic agent, Expert Opin. Ther. Targets 20 (2016) 1–5, https://doi.org/10.1517/14728222.2016.1093114.
[16] S. Chakrabortty, M. Sison, Y. Wu, A. Ladenburger, G. Pramanik, J. Biskupek, J. Extermann, U. Kaiser, T. Lasser, T. Weil, NIR-emitting and photo-thermal active nanogold as mitochondria-specific probes, Biomater. Sci. 5 (2017) 966–971, https://doi.org/10.1039/c6bm00951d.
[17] P. Liu, Y. Wang, Y. Liu, F. Tan, J. Li, N. Li, S-nitrosothiols loaded mini-sized Au@silica nanorod elicits collagen depletion and mitochondrial damage in solid tumor treatment, Theranostics 10 (2020) 6774–6789, https://doi.org/10.7150/thno.42661.
[18] J. Ingle, B. Uttam, R. Panigrahi, S. Khatua, S. Basu, Dog-bone shaped gold nanoparticle-mediated chemo-photothermal therapy impairs the powerhouse to trigger apoptosis in cancer cells, J. Mater. Chem. B B. 11 (2023) 9732–9741, https://doi.org/10.1039/d3tb01716h.
[19] G. Qi, Y. Zhang, S. Xu, C. Li, D. Wang, H. Li, Y. Jin, Nucleus and mitochondria targeting theranostic plasmonic surface-enhanced Raman spectroscopy nanoprobes as a means for revealing molecular stress response differences in hyperthermia cell death between cancerous and normal cells, Anal. Chem. 90 (2018) 13356–13364, https://doi.org/10.1021/acs.analchem.8b03034.
[20] M.M. Mkandawire, M. Lakatos, A. Springer, A. Clemens, D. Appelhans, U. Krause-Buchholz, W. Pompe, G. Rödel, M. Mkandawire, Induction of apoptosis in human cancer cells by targeting mitochondria with gold nanoparticles, Nanoscale 7 (2015) 10634–10640, https://doi.org/10.1039/c5nr01483b.
[21] F.M. Chen, L.J. Huang, F. Ou-Yang, J.Y. Kan, L.C. Kao, M.F. Hou, Activation of mitochondrial unfolded protein response is associated with Her2-overexpression breast cancer, Breast Cancer Res. Treat. 183 (2020) 61–70, https://doi.org/10.1007/s10549-020-05729-9.
[22] G. Alberti, G. Vergilio, L. Paladino, R. Barone, F. Cappello, E. Conway de Macario, A.J.L. Macario, F. Bucchieri, F. Rappa, The chaperone system in breast cancer: roles and therapeutic prospects of the molecular chaperones Hsp27, Hsp60, Hsp70, and Hsp90, Int. J. Mol. Sci. 23 (2022) 7792, https://doi.org/10.3390/ijms23147792.
[23] J. Saini, P.K. Sharma, Clinical, prognostic and therapeutic significance of heat shock proteins in cancer, Curr. Drug Targets 19 (2018) 1478–1490, https://doi.org/10.2174/1389450118666170823121248.
[24] F. Cappello, E. Conway de Macario, L. Marasà, G. Zummo, A.J. Macario, Hsp60 expression, new locations, functions and perspectives for cancer diagnosis and therapy, Cancer Biol. Ther. 7 (2008) 801–809, https://doi.org/10.4161/cbt.7.6.6281.
[25] S. Yang, J. Meng, Y. Yang, H. Liu, C. Wang, J. Liu, Y. Zhang, C. Wang, H. Xu, A HSP60-targeting peptide for cell apoptosis imaging, Oncogenesis 5 (2016) e201, https://doi.org/10.1038/oncsis.2016.14.
[26] T. Wen, Z. Hu, W. Liu, H. Zhang, S. Hou, X. Hu, X. Wu, Copper-ion-assisted growth of gold nanorods in seed-mediated growth: significant narrowing of size distribution via tailoring reactivity of seeds, Langmuir 28 (2012) 17517–17523, https://doi.org/10.1021/la304181k.
[27] W. Zhang, Y. Ji, J. Meng, X. Wu, H. Xu, Probing the behaviors of gold nanorods in metastatic breast cancer cells based on UV-vis-NIR absorption spectroscopy, PLoS One 7 (2012) e31957, https://doi.org/10.1371/journal.pone.0031957.
[28] W.H. Lei, H.X. Liu, L.J. Zhong, X.D. Yang, K. Wang, Vanadyl ions binding to GroEL (HSP60) and inducing its depolymerization, Chin. Sci. Bull. 52 (2007) 2775–2781, https://doi.org/10.1007/s11434-007-0380-0.
[29] R. Zhao, R. Zhang, L. Feng, Y. Dong, J. Zhou, S. Qu, S. Gai, D. Yang, H. Ding, P. Yang, Constructing virus-like SiO(x)/CeO(2)/VO(x) nanozymes for 1064 nm light-triggered mild-temperature photothermal therapy and nanozyme catalytic therapy, Nanoscale 14 (2022) 361–372, https://doi.org/10.1039/d1nr06128c.

[30] H.O. Barazi, L. Zhou, N.S. Templeton, H.C. Krutzsch, D.D. Roberts, Identification of heat shock protein 60 as a molecular mediator of alpha 3 beta 1 integrin activation, Cancer Res. 62 (2002) 1541–1548.
[31] R.P. Miskin, J.S.A. Warren, A. Ndoye, L. Wu, J.M. Lamar, C.M. DiPersio, Integrin α3β1 promotes invasive and metastatic properties of breast cancer cells through induction of the brn-2 transcription factor, Cancers 13 (2021) 480, https://doi.org/10.3390/cancers13030480.
[32] E.M. Bolitho, C. Sanchez-Cano, H. Shi, P.D. Quinn, M. Harkiolaki, C. Imberti, P. J. Sadler, Single-cell chemistry of photoactivatable platinum anticancer complexes, J. Am. Chem. Soc. 143 (2021) 20224–20240, https://doi.org/10.1021/jacs.1c08630.
[33] Y. Kim, C. Kim, O.Y. Kwon, D. Nam, S.S. Kim, J.H. Park, S. Kim, M. Gallagher-Jones, Y. Kohmura, T. Ishikawa, C. Song, G. Tae, D.Y. Noh, Visualization of a mammalian mitochondrion by coherent X-ray diffractive imaging, Sci. Rep. 7 (2017) 1850, https://doi.org/10.1038/s41598-017-01833-x.
[34] M.A. Le Gros, G. McDermott, C.A. Larabell, X-ray tomography of whole cells, Curr. Opin. Struct. Biol. 15 (2005) 593–600, https://doi.org/10.1016/j.sbi.2005.08.008.
[35] M. Uchida, Y. Sun, G. McDermott, C. Knoechel, M.A. Le Gros, D. Parkinson, D. G. Drubin, C.A. Larabell, Quantitative analysis of yeast internal architecture using soft X-ray tomography, Yeast 28 (2011) 227–236, https://doi.org/10.1002/yea.1834.
[36] I. Manoli, S. Alesci, M.R. Blackman, Y.A. Su, O.M. Rennert, G.P. Chrousos, Mitochondria as key components of the stress response, Trends Endocrinol. Metabol. 18 (2007) 190–198, https://doi.org/10.1016/j.tem.2007.04.004.
[37] J. Ren, J. Zhou, H. Liu, X. Jiao, Y. Cao, Z. Xu, Y. Kang, P. Xue, Ultrasound (US)-activated redox dyshomeostasis therapy reinforced by immunogenic cell death (ICD) through a mitochondrial targeting liposomal nanosystem, Theranostics 11 (2021) 9470–9491, https://doi.org/10.7150/thno.62984.
[38] J. Wan, X. Zhang, Z. Li, F. Mo, D. Tang, H. Xiao, J. Wang, G. Rong, T. Liu, Oxidative stress amplifiers as immunogenic cell death nanoinducers disrupting mitochondrial redox homeostasis for cancer immunotherapy, Adv. Healthcare Mater. 12 (2023) e2202710, https://doi.org/10.1002/adhm.202202710.
[39] S.A. DuPre, K.W. Hunter Jr., Murine mammary carcinoma 4T1 induces a leukemoid reaction with splenomegaly: association with tumor-derived growth factors, Exp. Mol. Pathol. 82 (2007) 12–24, https://doi.org/10.1016/j.yexmp.2006.06.007.
[40] S. Parveen, S. Siddharth, L.S. Cheung, A. Kumar, J. Shen, J.R. Murphy, D. Sharma, W.R. Bishai, Therapeutic targeting with DABIL-4 depletes myeloid suppressor cells in 4T1 triple-negative breast cancer model, Mol. Oncol. 15 (2021) 1330–1344, https://doi.org/10.1002/1878-0261.12938.
[41] H. Zheng, S. Siddharth, S. Parida, X. Wu, D. Sharma, Tumor microenvironment: key players in triple negative breast cancer immunomodulation, Cancers 13 (2021) 3357, https://doi.org/10.3390/cancers13133357.
[42] Y. Lv, F. Li, S. Wang, G. Lu, W. Bao, Y. Wang, Z. Tian, W. Wei, G. Ma, Near-infrared light-triggered platelet arsenal for combined photothermal-immunotherapy against cancer, Sci. Adv. 7 (2021) eabd7614, https://doi.org/10.1126/sciadv.abd7614.
[43] J. Meng, J. Meng, J. Duan, H. Kong, L. Li, C. Wang, S. Xie, S. Chen, N. Gu, H. Xu, X. D. Yang, Carbon nanotubes conjugated to tumor lysate protein enhance the efficacy of an antitumor immunotherapy, Small 4 (2008) 1364–1370, https://doi.org/10.1002/smll.200701059.
[44] Q. Meng, B.X. Li, X. Xiao, Toward developing chemical modulators of Hsp60 as potential therapeutics, Front. Mol. Biosci. 5 (2018) 35, https://doi.org/10.3389/fmolb.2018.00035.
[45] Y. Tang, Y. Zhou, S. Fan, Q. Wen, The multiple roles and therapeutic potential of HSP60 in cancer, Biochem. Pharmacol. 201 (2022) 115096, https://doi.org/10.1016/j.bcp.2022.115096.
[46] M.M.W.H.J. Liu, X.X. Hu, S.S. Shi, P.S. Xu, Enhanced photothermal therapy through the in situ activation of a temperature and redox dual-sensitive nanoreservoir of triptolide, Small 16 (2020) 2003398.
[47] A. Ndoye, R.P. Miskin, C.M. DiPersio, Integrin α3β1 represses reelin expression in breast cancer cells to promote invasion, Cancers 13 (2021) 344, https://doi.org/10.3390/cancers13020344.
[48] G. Kroemer, L. Galluzzi, O. Kepp, L. Zitvogel, Immunogenic cell death in cancer therapy, Annu. Rev. Immunol. 31 (2013) 51–72, https://doi.org/10.1146/annurev-immunol-032712-100008.
[49] D.V. Krysko, A.D. Garg, A. Kaczmarek, O. Krysko, P. Agostinis, P. Vandenabeele, Immunogenic cell death and DAMPs in cancer therapy, Nat. Rev. Cancer 12 (2012) 860–875, https://doi.org/10.1038/nrc3380.
[50] Y. Li, H. Zhang, Y. Merkher, L. Chen, N. Liu, S. Leonov, Y. Chen, Recent advances in therapeutic strategies for triple-negative breast cancer, J. Hematol. Oncol. 15 (2022) 121, https://doi.org/10.1186/s13045-022-01341-0.